my journal manuscript No.
(will be inserted by the editor)

Magnetic Helicity, Tilt, and Twist.

Alexei A. Pevtsov · Mitchell A. Berger · Alexander Nindos · Aimee A. Norton · Lidia van Driel-Gesztelyi

Received: date / Accepted: date

Abstract Since its introduction to astro- and solar physics, the concept of helicity has proven to be useful in providing critical insights into physics of various processes from astrophysical dynamos, to magnetic reconnection and eruptive phenomena. Signature of helicity was also detected in many solar features, including orientation of solar active regions, or Joy's law. Here we provide a summary of both solar phenomena and consider mutual relationship and its importance for the evolution of solar magnetic fields.

Keywords Helicity · Joy's Law · Magnetic Field

1 Introduction

This article deals with two seemingly unlike phenomena: (magnetic, current) helicity and the orientation of solar active regions (Joy's Law). Joy's law represents one of the earliest observational tendencies discovered at the beginning of modern era of solar observations (Hale et al. 1919), while helicity is a more recent subject (Berger and Field 1984; Seehafer 1990; Martin et al. 1994; Pevtsov

A.A. Pevtsov
National Solar Observatory, USA
Tel.: +157-54-347011
Fax: +157-54-347029
E-mail: apevtsov@nso.edu

M.A. Berger
University of Exeter, U.K.

A. Nindos
University of Ioannina, Greece

A.A. Norton
Stanford University, USA

L. van Driel-Gesztelyi
University College London, U.K.

et al. 1994; Rust 1994). But are these two phenomena completely unrelated? Here we present overview of recent studies of helicity and Joy's law, investigate their possible relation, and discuss what the relation between helicity and active region tilt may tell us about the origin and the evolution of magnetic fields on the Sun.

Early studies of helicity on the Sun are well-represented by individual articles in Brown et al. (1999). Later developments were described in Büchner and Pevtsov (2003). A graphic summary of the hemispheric helicity rule encompassing magnetic fields on spatial scales from quiet Sun network to the interplanetary magnetic field was presented in Pevtsov (2002). A more recent update on the hemispheric helicity rule can be found in Pevtsov (2008). Some details omitted from the present article can be found in these earlier reviews.

The rest of the article is organized as follows. Section 2 presents a summary of the theoretical basis of the helicity concept. Sections 3–5 present an overview of the current observations of helicity on the Sun and the heliosphere. Section 6 considers different aspects relevant to orientation of solar active region (Joy's Law), and Section 7 summarizes the article.

2 Basic Theory

Magnetic helicity is a measure of important structural properties of a magnetic field such as twist, shear, linking, and kinking. It is conserved to an excellent approximation in the highly conducting plasmas present in the Sun and heliosphere. The large magnetic Reynolds numbers (10^8 to 10^{15}) in the solar corona produce ideal magnetohydrodynamic (MHD) behaviour on large scales. Resistive MHD processes on smaller scales (current sheet formations and magnetic reconnection) barely affect the conservation of total magnetic helicity (Berger 1984). Any detailed model of the Sun and heliosphere, in order to be consistent, must obey the helicity balance equations. In this sense, magnetic helicity can be considered a more robust invariant than total energy, as ideal motions convert energy back and forth between kinetic and magnetic forms, dissipative processes convert both forms into heat, and various plasma processes convert energy into particle acceleration.

Although magnetic helicity is conserved, it can be transported between regions; in addition helicity can be transferred between different length-scales. Helicity transport between regions obeys a Poynting-like equation; it involves either the bulk transfer of a helicity-carrying field from one region to the other, or propagation of twist and braiding along field lines crossing the boundary between the regions (Berger and Field 1984; Pariat et al. 2006).

We can distinguish two types of scale transfers. First, when there is a net helicity of one sign, there is a tendency for turbulent plasma to generate or maintain a large-scale magnetic field structure via the inverse cascade of magnetic helicity to longer wavelengths. Secondly, ideal processes can generate large-scale helicity of one sign balanced by small-scale helicity of the opposite sign. Thus a magnetic flux rope rising through the convection zone can kink

due to Coriolis forces. The kinking (measured as *writhe*) represents large scale helicity of one sign, balanced by a small scale helicity (internal twisting of field lines) of the opposite sign.

Helicity affects the solar cycle and activity in several ways. First, in the interior of the Sun, the solar dynamo is responsible for regeneration of the magnetic field and the 11-year solar cycle. Differential rotation provides an essential contribution to the dynamo; the effect of differential rotation on the magnetic field can be directly quantified using magnetic helicity techniques (Berger and Ruzmaikin 2000). On the other hand, too much helicity can suppress turbulent dynamo (alpha effect) action.

Secondly, magnetic helicity build-up in a solar active region can lead to enhanced activity. Of particular importance for the space weather effects and forecasting potential is the realisation that increasing the pinch or helicity content in a solar filament or an active region can also increase the probability of eruption eruption (e.g., Romano and Zuccarello 2011).

Third, if we go further into the heliosphere, helicity can also play an important role. The helicity of filaments and active regions can be examined before an eruption; after the eruption, this helicity can be compared to that of the remaining active region and of the corresponding magnetic cloud (e.g. Foullon et al. 2007).

Here we detail how helicity and helicity transport can be calculated, and how it relates to structural features of a magnetic field such as twist, kinking, and linking.

2.1 Linking, twisting, and helicity integrals

Magnetic helicity integrals measure the net interlinking and twisting of magnetic field lines. Before thinking about magnetic fields in general, consider two simple cases: first, where the field-lines are all closed curves; and second, where the field-lines extend between parallel planes. In the first case, the helicity measures the net linking between all pairs of field-lines. In the second, the helicity measures the net twist between all pairs of field-lines. Of course, the number of field-lines in a magnetised volume is infinite, so the sums over linking and winding are weighted by magnetic flux.

The Gauss linking number (Ricca and Nipoti 2011) is a double line integral along two closed curves (see figure 1). This integral gives an integer, as long as the two curves are distinct (when they are the same curve, it gives the *writhe* as discussed below). The magnetic field counterpart of the linking number is the closed magnetic helicity.

Let σ and τ parametrize curves 1 and 2, and label points on these curves as $\mathbf{x}(\sigma)$ and $\mathbf{y}(\tau)$. Also let $\mathbf{r} = \mathbf{y} - \mathbf{x}$. The Gauss linking number is

$$L_{12} = -\frac{1}{4\pi} \oint_1 \oint_2 \frac{d\mathbf{x}}{d\sigma} \cdot \frac{\mathbf{r}}{r^3} \times \frac{d\mathbf{y}}{d\tau} \, d\tau \, d\sigma. \tag{1}$$

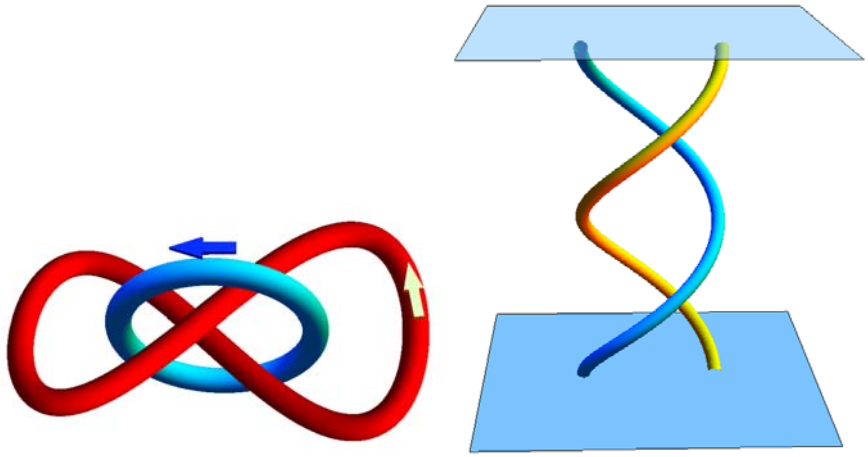

Fig. 1 Left: If these were magnetic flux tubes with net axial fluxes Φ_1 and Φ_2, then the helicity would be $H = 2L\Phi_1\Phi_2 + T_1\Phi_1^2 + T_2\Phi_2^2$ where T_1 and T_2 measure the net twisting of field lines within the tubes about their axes. For these tubes, the linking number is $L = 2$. Right: two tubes stretched between parallel planes. Here $H = 2w\Phi_1\Phi_2 + T_1\Phi_1^2 + T_2\Phi_2^2$, where w is their winding number. For the tubes shown, the winding number $w = 1$.

The magnetic field counterpart is a double volume integral in a volume $\mathcal{V}$ with boundary S. Assuming the field is closed within the volume (i.e. $\mathbf{B}\cdot\hat{n} = 0$ at the boundary S) we have the magnetic helicity (Moffatt 1969)

$$H = -\frac{1}{4\pi}\int\int \mathbf{B}(\mathbf{x})\cdot\frac{\mathbf{r}}{r^3}\times\mathbf{B}(\mathbf{y})\ \mathrm{d}^3x\, d^3y. \tag{2}$$

This double integral form of the helicity provides an important caution: helicity is a non-local quantity; it does not have a simple density like mass. However, this form is unwieldy and difficult to use. To simplify calculations, employ the Coulomb gauge vector potential

$$\mathbf{A}(\mathbf{x}) = -\frac{1}{4\pi}\int \frac{\mathbf{r}}{r^3}\times\mathbf{B}(\mathbf{y})\, d^3y, \tag{3}$$

which gives magnetic helicity the more widely known form (for a closed volume)

$$H = \int \mathbf{A}\cdot\mathbf{B}\ \mathrm{d}^3x. \tag{4}$$

Note, however, that gauge transformations of $\mathbf{A}$ may change the value of this integral when magnetic flux crosses the boundary (and also if the volume is multiply-connected, Berger 1999).

For magnetically open or multiply connected volumes (where $\mathbf{B}\cdot\hat{n} \neq 0$ at the boundary S), we measure helicity relative to some field with minimum structure. Let $\mathbf{B}_{pot}$ be the potential field in $\mathcal{V}$. Suppose the total magnetic field $\mathbf{B}_{tot}$ in all space (including $\mathcal{V}$ and its complement outside of $\mathcal{V}$) vanishes

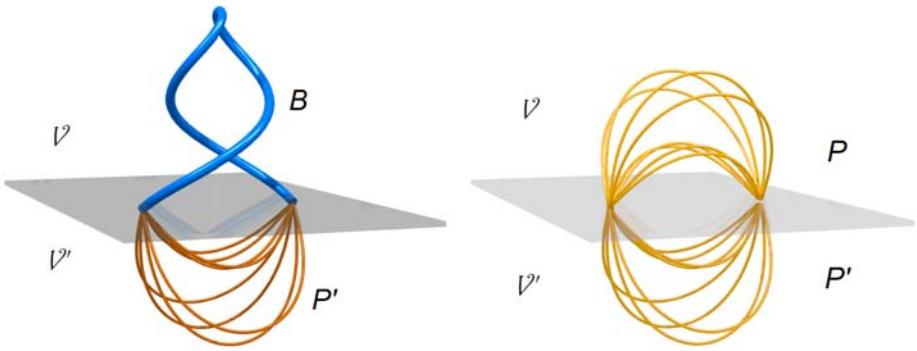

Fig. 2 Left: We wish to define the helicity of the open field in the upper part ($\mathcal{V}$) of the left figure. To accomplish this, we extend the field to the volume $\mathcal{V}'$ below the boundary. Let the total helicity, as measured by equation 4 be H_{tot}. Next, replace $\mathbf{B}$ in $\mathcal{V}$ by its corresponding potential field $\mathbf{B}_{pot}$; the helicity of this reference field (with the field inside $\mathcal{V}'$ unchanged) is H_{ref}. The relative helicity is then $H_{tot} - H_{ref}$.

at infinity, so that its helicity $H(\mathbf{B}_{tot})$ is finite. Then (Berger and Field 1984) we can define a reference field $\mathbf{B}_{ref}$ which is the same as $\mathbf{B}_{tot}$ outside of $\mathcal{V}$ but equals the potential field $\mathbf{P}$ inside (figure 2). We then define the helicity inside the volume $\mathcal{V}$ to be

$$H(\mathcal{V}) = H(\mathbf{B}_{tot}) - H(\mathbf{B}_{ref}), \tag{5}$$

with helicities calculated using equation 4. This helicity only depends on what is happening inside $\mathcal{V}$; one can show (Berger and Field 1984; Finn and Antonsen 1983)

$$H(\mathcal{V}) = \int (\mathbf{A} + \mathbf{A}_{pot}) \cdot (\mathbf{B} - \mathbf{B}_{pot}) \, \mathrm{d}^3x. \tag{6}$$

This generalized helicity can be shown to be gauge invariant for any boundary conditions or topology of the boundary S.

If the volume $\mathcal{V}$ lies between two planes, and all field lines stretch between the boundaries, then the helicity is a sum of winding numbers between the planes, as in figure 1, right. For other configurations, the interpretation can become more complicated. For most solar atmospheric problems, a more appropriate geometry would be loops with footpoints on a sphere (or at least a plane). Again the helicity measures the net amount the loops wind about each other. In addition, for a sheared arcade, the helicity will be related to the amount of shear. A detailed account of calculating the helicity of loops is given in Pariat et al. (2006).

2.2 Poloidal and toroidal fields

In Cartesian or spherical geometries it is often useful to decompose a magnetic field into toroidal and poloidal components. Solar dynamo action is often described in terms of differential rotation acting on a poloidal field to regenerate

the toroidal field (the *omega* effect), along with helical turbulence acting on the toroidal field to regenerate the poloidal field (the *alpha* effect, Charbonneau 2005).

Let $\mathcal{L}$ be the operator

$$\mathcal{L} \equiv \begin{cases} -\hat{z} \times \nabla, \text{ Cartesian geometry;} \\ -\mathbf{r} \times \nabla, \text{ Spherical geometry.} \end{cases} \tag{7}$$

Then we can write

$$\mathbf{B} = \mathcal{L}T + \nabla \times \mathcal{L}P, \tag{8}$$

where T is the toroidal function and P is the poloidal function.

The operator $\mathcal{L}$ has two important properties: first, it's divergence vanishes,

$$\nabla \cdot \mathcal{L} = 0. \tag{9}$$

Secondly, it is transverse:

$$\begin{array}{l} \hat{z} \cdot \mathcal{L} = 0, \text{ Cartesian geometry;} \\ \mathbf{r} \cdot \mathcal{L} = 0, \text{ Spherical geometry.} \end{array} \tag{10}$$

The vector potentials of the toroidal field $\mathbf{B}_T = \mathcal{L}T$ and the poloidal field $\mathbf{B}_P = \nabla \times \mathcal{L}P$ are

$$\mathbf{A}_T = T\hat{z} + \nabla\Psi_T; \tag{11}$$

$$\mathbf{A}_P = \mathcal{L}P + \nabla\Psi_P. \tag{12}$$

where $\Psi_T(x, y, z)$ and $\Psi_P(x, y, z)$ are gauge functions.

The functions P and T can be obtained from $\mathbf{B}$ by solving the equations

$$\frac{\partial^2 P}{\partial x^2} + \frac{\partial^2 P}{\partial y^2} = B_z; \tag{13}$$

$$\frac{\partial^2 T}{\partial x^2} + \frac{\partial^2 T}{\partial y^2} = (\nabla \times \mathbf{B})_z. \tag{14}$$

Theorem

Consider a magnetic field $\mathbf{B} = \mathbf{B}_T + \mathbf{B}_P$ in a region $\mathcal{V}$. Assume that $\mathcal{V}$ is either 1) all space, 2) a half space bounded by a plane, 3) a layer bounded by two planes, 4) the interior or exterior of a sphere, or 5) a spherical shell bounded by two concentric spheres. Then

1. A purely poloidal field ($T = 0$) has helicity $H = 0$.
2. A purely toroidal field ($P = 0$) has helicity $H = 0$.
3. In general,

$$H(\mathbf{B}) = 2 \int_{\mathcal{V}} \mathcal{L}T \cdot \mathcal{L}P \, \mathrm{d}^3x. \tag{15}$$

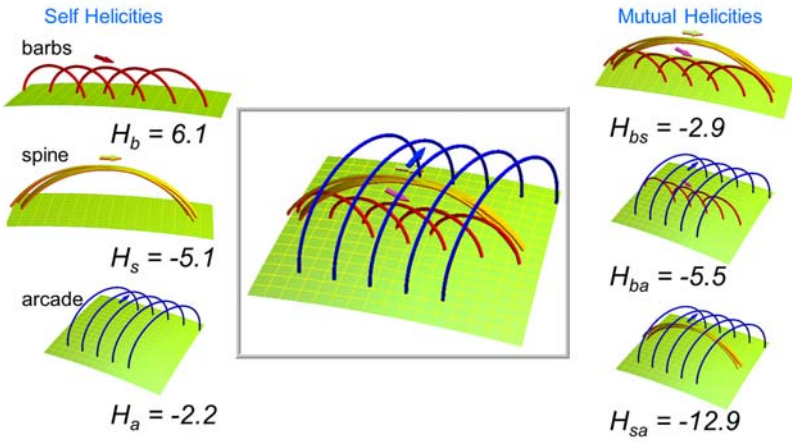

Fig. 3 A cartoon model of a prominence magnetic field, based on Martin et al. (2012). The magnetic flux has been divided into distinct regions corresponding to arcade fields on top, the axis field going all the way along the prominence, and barb fields below. Each single flux element shown has one unit of flux. The self helicities of each region are shown on the left, while their mutual helicities are shown on the right.

These results follow from the definitions of helicity and relative helicity, and equations 9 and 10. Here we give an outline of the proof in a Cartesian geometry. As the helicity integrals are gauge invariant, we can ignore gauge functions Ψ_P and Ψ_T. For a purely toroidal field

$$\int \mathbf{A}_T \cdot \mathbf{B}_T \, \mathrm{d}^3x = \int T\hat{z} \cdot \mathcal{L}T \, \mathrm{d}^3x = 0. \tag{16}$$

For purely poloidal fields, there is somewhat more work:

$$\begin{aligned} \int \mathcal{L}P \cdot \mathbf{B}_P \, \mathrm{d}^3x &= \int (\nabla \times P\hat{z}) \cdot \left(\nabla \frac{\partial P}{\partial z} - \hat{z}\nabla^2 P \right) \, \mathrm{d}^3x \\ &= \int \nabla \cdot P\hat{z} \times \nabla \frac{\partial P}{\partial z} \, \mathrm{d}^3x = \oint \hat{z} \cdot P\hat{z} \times \nabla \frac{\partial P}{\partial z} \, \mathrm{d}^2x \\ &= 0. \end{aligned} \tag{17}$$

For a field containing both toroidal and poloidal components, only the cross-terms give non-zero results. There will be two of these, corresponding to $\mathbf{A}_T \cdot \mathbf{B}_P$ and $\mathbf{A}_P \cdot \mathbf{B}_T$, but both reduce to the integral of $\mathcal{L}P \cdot \mathcal{L}T$. When calculating relative helicities, the same results apply (note that the potential field is purely poloidal).

2.3 Self and mutual helicity

Suppose we divide the magnetic field in a volume $\mathcal{V}$ into two or more distinct components, with the proviso that any individual field line stays entirely

within one component. Recall that helicity can be described as a sum or integral over the linking or twist numbers of all pairs of field lines. Then we can ask what happens when we restrict the sum to pairs where both lines stay belong to one component. In this case we obtain the *self-helicity* of the component. If we look at all pairs where one line is in one component and a second line is in another component, then we obtain the *mutual helicity* between the two components. For example, figure 3 shows a cartoon of a prominence field (Martin et al. 2012), divided into components: an overlying arcade, the field along the filament axis, and low-lying barbs connecting the filament with the field below. Each component can have its own self-helicity due to its internal twist and shear. In addition, two different components will share a mutual helicity due to their interlinking or shear.

Reconnection between two components of a field can exchange self and mutual helicities, while keeping the total helicity approximately conserved. For example, consider a simple reconnection of two equal flux tubes of flux Φ. The mutual helicity of the new tubes will differ from that of the old tubes by $\Delta H_{mutual} = \pm\Phi^2$. In a simple reconnection (with one reconnection site, the final tubes will share this helicity equally, both obtaining a half twist $\Delta H_{self} = \pm\frac{1}{2}\Phi^2$ as a result (Wright and Berger 1989). Such sudden acquisitions of half twists may be observable. For example, a recent force-free modelling of an active region corona using vector SDO/HMI magnetograms (Thalmann et al. 2014) displays an apparent increase of a half turn twist in a flux rope.

Often in solar physics and MHD theory one considers individual flux ropes, for example an x-ray loop with footpoints on the photosphere. Let the coronal volume (here anything exterior to the photosphere) be denoted by $\mathcal{V}_c$. Suppose a particular flux rope occupies a volume $\mathcal{V}_r$ inside $\mathcal{V}_c$. There are a few ways of calculating the self-helicity of the rope. The self helicity should give the sum of twist inside the rope, plus the writhe of the rope's axis (see below). If we calculate the relative helicity of the rope volume $\mathcal{V}_c$ alone, we will obtain only the twist due to axial currents inside the rope, losing the writhe altogether (for example, if there are no currents inside the volume (potential field of $\mathcal{V}_c$) then the relative helicity $H(\mathcal{V}_c) = 0$). Alternatively, one could calculate the relative helicity of the entire corona, i.e. $H(\mathcal{V}_c)$, but with $\mathbf{B}$ set to 0 outside the rope. This will give the sum of twist and writhe. Detailed methods for calculating helicities of individual ropes or subvolumes are given in Low (2006); Longcope and Malanushenko (2008). These methods are especially useful when considering partial relaxation of a field to a piece-wise linear force free field.

2.4 Twist and Writhe

The self helicity of a flux tube can take two forms, *twist* and *writhe*: $H = Tw + Wr$ (Călugăreanu 1961; Moffatt and Ricca 1992; Berger and Prior 2006; Török et al. 2010). The writhe measures the winding and kinking of the axis, but is not itself a topological or ideal invariant. The concept of writhe is

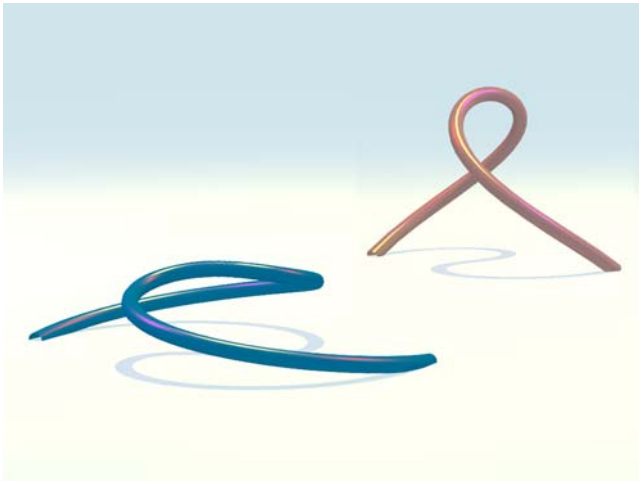

Fig. 4 Two flux ropes. Both ropes have an inverse S shape as seen in projection. However, the one on the left has a writhe writhe $W_r = -0.2\Phi^2$ while the rope on the right has writhe $W_r = +0.2\Phi^2$. This demonstrates that a low lying loop can have the opposite sign of writhe to a taller loop with the same projection curve.

commonly used in biochemistry: DNA molecules must be highly coiled in order to fit inside the nucleus of a cell, and hence exhibit a very large value of Wr.

Writhe measures helical structure of the axis of a loop, but cannot be computed from the projection of the loop on the photosphere alone (see figure 4); the height of the loop is also important. During a kink instability, a twisted flux rope may convert some of its twist to writhe. Unfortunately, the amount of twist contained in the rope before the eruption cannot be accurately inferred from observing the amount of writhe produced by this conversion (Török et al. 2014). The amount of writhe produced depends mainly on the details of the instability, rather than the initial twist.

2.5 Magnetic helicity transport

We wish to give a simple expression for dH/dt, which may include both dissipation and transport across boundaries. Although we may use any gauges we please for $\mathbf{A}$ and $\mathbf{A}_{pot}$, one particular choice considerably simplifies the algebra (Berger 1984). First, we require that $\mathbf{A}_{pot}$ satisfies

$$\nabla \cdot \mathbf{A}_{pot} = 0; \qquad \mathbf{A}_{pot} \cdot \hat{\mathbf{n}}|_S = 0. \tag{18}$$

One then finds

$$\frac{\mathrm{d}H}{\mathrm{d}t} = -2 \int \mathbf{E} \cdot \mathbf{B} \ \mathrm{d}^3x + 2 \oint_S \mathbf{A}_{pot} \times \mathbf{E} \cdot \hat{\mathbf{n}} \mathrm{d}S, \tag{19}$$

where $\mathbf{E}$ is the electric field. This equation is analogous to Poynting's theorem for the dissipation and transport of electromagnetic energy. The first term

corresponds to dissipation; magnetic helicity dissipation can be shown to be negligible in high magnetic Reynolds number plasmas (Berger 1984; Ortolani and Schnack 1993).

The second term governs transport across the boundary S. For the photosphere, the dominant contribution to $\mathbf{E}$ comes from ideal MHD flow. In this case $\mathbf{E} = \mathbf{B} \times \mathbf{V}$ (also see, Berger 1984)

$$\frac{\mathrm{d}H}{\mathrm{d}t} = 2 \oint_S \left((\mathbf{A}_{pot} \cdot \mathbf{V})\mathbf{B} - (\mathbf{A}_{pot} \cdot \mathbf{B})\mathbf{V} \right) \cdot \hat{\mathbf{n}} \mathrm{d}S. \tag{20}$$

The first term represents the effect of twisting motions on the boundary, while the second represents the bulk transport of helical field across the boundary.

The helicity transport equation takes an intuitive form in the simple case where N flux tubes pass through a planar boundary. Let flux tube i have flux Φ_i. Suppose the motion at boundary rotates flux tube i at an angular velocity ω_{ii}, while tube i and tube j rotate about each other at an angular velocity ω_{ij}. Then

$$\frac{\mathrm{d}H}{\mathrm{d}t} = \frac{1}{2\pi} \sum_{i=1}^{N} \sum_{j=1}^{N} \omega_{ij} \Phi_i \Phi_j. \tag{21}$$

3 Computations of helicity in finite volumes

3.1 Computations of instantaneous helicity in the corona

The application of the concept of relative magnetic helicity defined in section 2 is problematic in active region (AR) magnetic field extrapolations because their volumes are finite. For linear force-free (LFF) fields, this problem can be bypassed by formulating the helicity content of an AR in terms of surface integrals applied to the lower boundary (Berger 1985; Georgoulis and LaBonte 2007). These calculations include summations over the Fourier modes of the magnetogram. When the force-free parameter α exceeds a certain critical value that depends on the horizontal size of the calculation box, helicity attains unphysical large values. Démoulin et al. (2002a) proposed to use the linearized Berger's (1985) expression in which the helicity is proportional to α. In several publications, (e.g. Démoulin et al. 2002a; Green et al. 2002; Nindos and Andrews 2004) the linearized formula has been used in conjunction with the single best value of α, α_{best}, for the AR (see section 3.3). In framework of LFF field, magnetic helicity can also be computed via α and magnetic energy, E_m (Pevtsov and Canfield 1999; Pevtsov 2008), with E_m determined from the Virial theorem.

Georgoulis et al. (2012) extended the work by Georgoulis and LaBonte (2007) on LFF fields to non-linear force-free (NLFF) fields. They developed a method that depends on a lower-boundary connectivity matrix that can be inferred either by a NLFF field extrapolation or in some other way. Instead of using extrapolation results, these authors used a unique connectivity-matrix

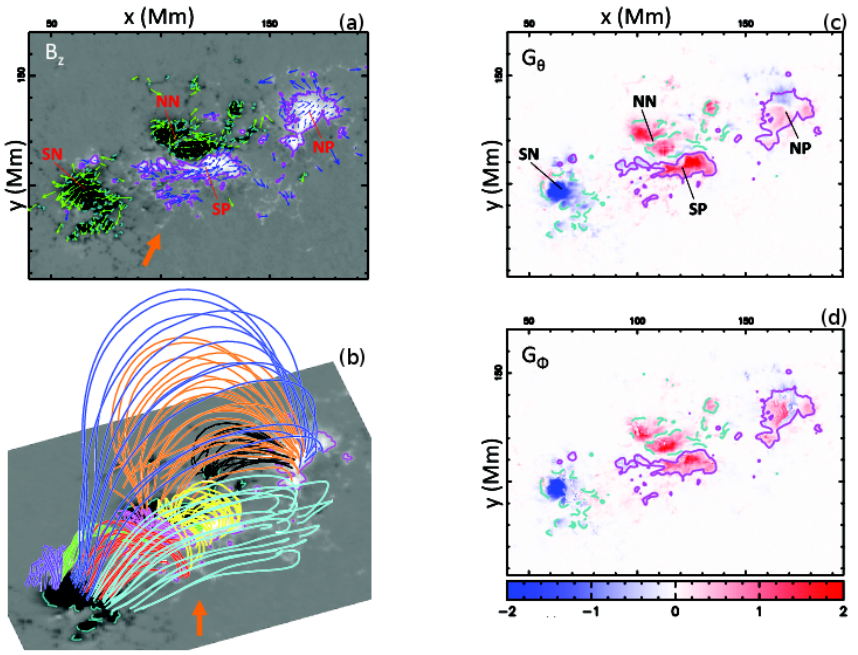

Fig. 5 AR11158 at 06:28 UT on 2011 February 14. (a) Photospheric vertical magnetic field, B_z, in grayscale overplotted with the flux transport velocity field (blue/green arrows) and the polarity labels. (b) 3D view of the NLFFF extrapolation with selected magnetic field lines. (c) G_θ map. (d) G_Φ map. In (c) and (d) the helicity flux density distributions are in units of 10^7 Wb^2 m^{-2} s^{-1} with the same color scale, and the $\pm$500 G isocontours of B_z are overplotted (modified from Dalmasse et al. 2013).

solution for a given flux-partition map. The solution relies on a simulated annealing algorithm designed to minimize the distances of connected opposite polarity partitions.

In several publications that treat the general problem of the calculation of the instantaneous helicity in the corona, NLFF field extrapolations are used, and the helicity in the computation box is estimated using methods that are based on the Coulomb gauge (e.g. Rudenko and Myshyakov 2011; Thalmann et al. 2011). The choice of gauge is irrelevant for the relative magnetic helicity value, but it may influence how computationally expensive the algorithm becomes. Valori et al. (2012) exploited the gauge freedom by choosing one that requires that one component of the vector potential vanishes; their method is a direct extension of an earlier work by DeVore (2000) to finite volumes.

3.2 Computations of the injection rate of helicity

When high-cadence photospheric magnetograms are available, the horizontal velocity related to equation 20 can be computed. In the early studies, several

authors (e.g. Chae 2001; Nindos and Zhang 2002; Moon et al. 2002a,b; Nindos et al. 2003; Chae et al. 2004) utilized the local correlation tracking (LCT) technique (November and Simon 1988) for the computation of horizontal velocities. Démoulin and Berger (2003) have pointed out that with magnetograms one follows the photospheric intersection of the magnetic flux tubes but not the evolution of the plasma. Consequently, from the observed magnetic evolution we obtain the flux tube motion and not the plasma motion parallel to the photosphere. If $\mathbf{v}_t$ is the tangential component of the photospheric plasma velocity and v_n the velocity perpendicular to the photosphere, the tracking algorithm detects the velocity of the footpoints of the flux tube which is

$$\mathbf{u} = \mathbf{v}_t - \frac{v_n}{B_n}\mathbf{B}_t \tag{22}$$

However, MHD simulations (Welsch et al. 2007) have shown that this formula is not always valid, and its use should be treated with caution especially during flux emergence episodes (see also Schuck 2008; Ravindra et al. 2008). This conclusion has been confirmed by Liu and Schuck (2012) who analyzed time series of HMI vector magnetograms from two emerging active regions (ARs).

The combination of equations 20 and 22 shows that the whole helicity flux density can be retrieved within the accuracy of the calculation. Consequently, one may use the quantity $G_A = -2\mathbf{u}\cdot\mathbf{A}_{pot}B_n$ as a proxy to the whole helicity flux density (e.g. Chae 2001; Nindos and Zhang 2002; Moon et al. 2002a,b; Nindos et al. 2003; Chae et al. 2004). The G_A maps always appear extremely complex both in space and time, with polarities of both signs present at any time. Pariat et al. (2005) showed that G_A is not a real helicity flux density and that its properties introduce artificial polarities of both signs. The spurious signals appear due to the fact that helicity flux density per unit surface is not physical quantity. Due to the properties of helicity, only helicity flux density per unit of elementary magnetic flux has a physical meaning. But to estimate such quantity using observations would require to isolate flux tubes and determine their connectivity, which is very difficult. Thus any definition of a helicity flux density will only be a proxy of the helicity flux density per unit magnetic flux. Pariat et al. (2005) introduced a new proxy for helicity flux density, G_θ, which does not suffer from G_A's problems. G_θ implies that the helicity injection rate is the summation of the rotation rate of all pairs of elementary fluxes weighted by their magnetic flux. An example of a G_θ map is given in figure 5(c).

In order to define the real helicity flux density, the coronal linkage needs to be provided. With it one can represent how all elementary flux tubes move relatively to a given elementary flux tube, and the helicity flux density is defined per elementary flux tube. Using photospheric maps this can be achieved by distributing equally the helicity input between the two footpoints for each elementary flux tube. Then the helicity flux can be rewritten as a flux of magnetic helicity per unit of surface, G_Φ, where G_Φ is a field-weighted average of G_θ at both photospheric footpoints, $\mathbf{x}_\pm$, of the photosheric connection.

While G_Φ provides the true helicity flux density, its practical use is presently limited by our ability to define the coronal linkage for all magnetic polarities. However, progress can be made if we obtain the coronal linkage from NLFFF extrapolations (Dalmasse et al. 2013, 2014). A G_Φ map resulted from such treatment appears in figure 5(d). This map corresponds to the same area whose G_θ map appears in figure 5(c).

It has been reported (e.g. Pariat et al. 2006, 2007) that unlike the usual G_A maps, most G_θ maps show almost unipolar spatial structures because the non-dominant helicity flux densities are significantly suppressed. However, as can be seen from figure 5(c), this is not always the case. In figure 5(d), the G_Φ map also displays mixed signals which implies that there are real mixed signs of the helicity flux in the AR. However, a comparison between figure 5(c) and figure 5(d) shows that the G_Φ distribution is different from the G_θ distribution, except in the regions of open magnetic fields (in these regions Dalmasse et al. 2013, set $G_\Phi = G_\theta$). Overall, the comparison shows that the intensity of the G_θ signal tends to be overestimated.

When a cube of helicity flux density maps is available, one can calculate the time evolution of the total helicity flux, dH/dt. An example using a time series of G_θ maps which includes the G_θ map of figure 5(c), appears in figure 6 (top panel, see Nindos et al. 2012). The resulting time profile of the net accumulated change of helicity is shown in the middle panel of figure 6. Note that we expect that the helicity flux integrated using G_A to be identical to the one integrated using G_θ or G_Φ because all definitions are derived from equation 20 (see Liu and Schuck 2013).

3.3 Computations of current helicity

Due to the difficulties involved in the computation of magnetic helicity, often proxies of the current helicity, H_c, are used instead. The current helicity is defined as $H_c = \int_V \mathbf{B} \cdot \mathbf{j} dV$, with $\mu_0 \mathbf{j} = \nabla \times \mathbf{B}$. While the magnetic helicity is gauge-dependent through $\mathbf{A}$, there is no gauge freedom with H_c ($\nabla \cdot \mathbf{B} = 0$). Furthermore, magnetic helicity is a conserved MHD quantity, but the current helicity is not. However, the magnetic and current helicity are usually considered to have the same sign (although this has not been proven rigorously). Observationally, we can derive values of the current helicity that represent only a fraction of its full value. This is because the volume integral of H_c can be written as $\int_V (B_x j_x + B_y j_y + B_z j_z) dV$, of which only the last component can be derived from observations. Though using photospheric vector magnetograms all three components of $\mathbf{B}$ are available, only the vertical component of $\mathbf{j}$ can be computed via the horizontal derivatives of $\mathbf{B}$. Therefore we can only determine a fraction of the whole current helicity density by calculating $h_c = B_z j_z$. Two different proxies based on current helicity have been used in statistical studies: the fractional imbalance of h_c (percentage of pixels of one sign of h_c in a given magnetogram) and area-averaged $h_c < h_c >$ (e.g. Abramenko et al. 1996; Bao and Zhang 1998). In sunspots, the horizontal components of $\mathbf{j}$

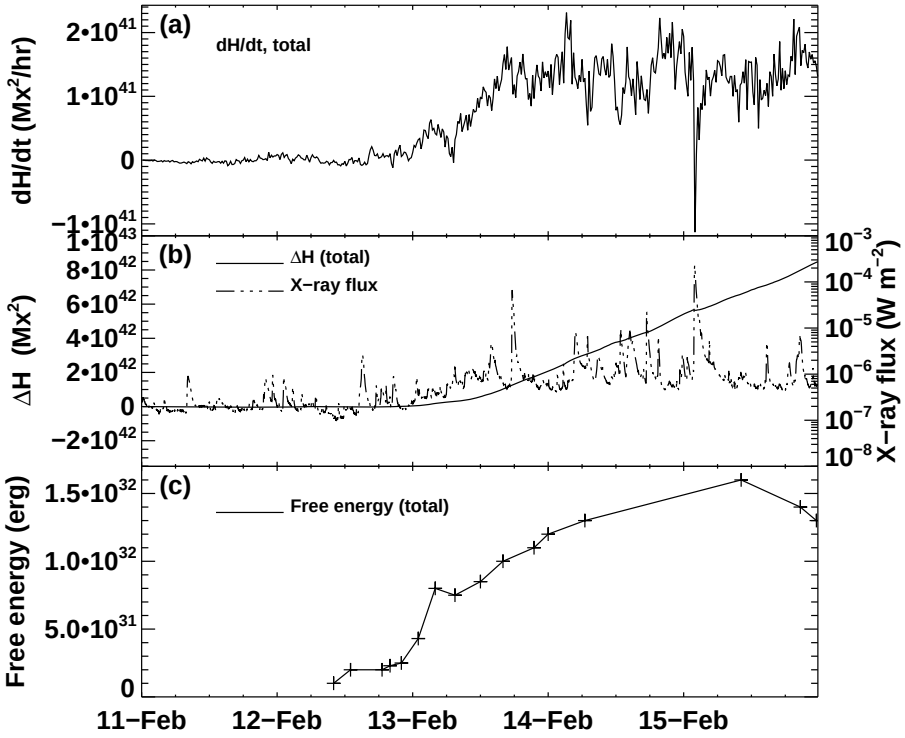

Fig. 6 (a) Time profile of the net flux of injected helicity, dH/dt, over the field of view of AR11158 that is presented in fig. 5(b) Time profile of the net accumulated change of helicity, ΔH, calculated from the measured dH/dt. The GOES soft X-ray flux time profile is also presented. (c) Temporal evolution of the magnetic free energy for AR11158 (modified from Nindos et al. 2012).

were determined either using the assumption of axisymmetric model (Pevtsov and Peregud 1990) or from the full Stokes polarimetric inversions on the basis of known difference in height formation of spectral line winds and core (Puschmann et al. 2010; Ruiz Cobo and Puschmann 2012). These studies indicated that the horizontal components of **j** may exceed significantly it vertical component.

One can also employ the value of the force-free field parameter α under the LFF approximation, as helicity proxy. Using photospheric vector magnetograms, one can determine α either by fitting LFF field to the observed transverse field (so called, α_{best}), or by computing the vertical component of α for each pixel and then averaging it ($< \alpha_z >$). Brunette et al. (2004) found a reasonably good correlation between α_{best} and $< \alpha_z >$. When longitudianl magnetograms are available instead of vector magnetograms, the α_{best} can be determined by comparing the computed LFF field lines with the observed soft X-ray or EUV coronal structures (e.g. Nindos and Andrews 2004). It has been shown (e.g., Hagyard and Pevtsov 1999) that helicity proxies h_c and α have the same sign.

4 Observations of magnetic helicity

4.1 Sources of magnetic helicity

The first term of the right-hand side of equation 20 corresponds to the injection of helicity by advection (i.e. emergence of field lines that cross the photosphere) while the second term (also known as shearing term) is the flux of helicity due to motions parallel to S (see section 3.2). Such motions may come either from differential rotation and/or transient photospheric shearing flows.

Differential rotation was the first mechanism considered that injects helicity into ARs (DeVore 2000). Even when a single bipole is considered, differential rotation does not provide a monotonous input of magnetic helicity (DeVore 2000). This is because differential rotation rotates both magnetic polarities on themselves and also changes their relative positions, introducing twist and writhe helicity fluxes, respectively. These fluxes always have opposite signs and similar amplitudes, and therefore partially cancel (Démoulin et al. 2002b). Démoulin et al. (2002a) and Green et al. (2002) studied the long-term evolution of the helicity injected by differential rotation into the coronal part of two active regions which were followed from their birth for several months during their decay. These studies showed that the contribution of differential rotation to the helicity budget of active regions remains small even on the long term.

However, the conclusion is different in the convection zone for a solar cycle and a global spatial scale. Berger and Ruzmaikin (2000) calculated the magnetic helicity production by differential rotation using 22 years of magnetogram data and differential rotation curves. They found that the helicity production in the solar interior by differential rotation had the correct sign compared to observations of coronal structures (the magnetic helicity conservation is satisfied by the natural generation of the same amount, but of opposite sign, in both hemispheres). The net helicity flow into each hemisphere over the whole 22-year magnetic cycle was about 4×10^{46} Mx^2.

ARs cover only a tiny fraction of the solar surface. The quiet Sun is characterized by small magnetic flux density but its total magnetic flux is huge. Welsch and Longcope (2003) estimated the helicity flux in five time series of quiet Sun magnetograms located close to disk center. They extrapolated their results to the whole Sun and found that the helicity injection in the quiet Sun is negligible compared to the helicity injected even by a single AR. We note, however, that their measurements included the braiding component only and therefore they should be considered as lower limits (the twist component of individual flux tubes was not measured because it was not possible to resolve tiny flux tubes).

The study of the helicity budget of active regions requires knowledge of the helicity injected into them and of the helicity carried away from them. The former is computed using the methods described in section 3 while CMEs are considered responsible for the latter. The helicity content of a CME can be estimated by the change of coronal helicity of the source region during the event (e.g. Mandrini et al. 2005; Tziotziou et al. 2013). Inside magnetic

clouds, helicity is estimated from modeling of the *insitu* measurements of the magnetic field vector. In practice, in studies of the long-term evolution of helicity of ARs that are linked to at least one magnetic cloud at 1 AU one assumes that the helicity carried away by each CME is equal to the helicity content in the magnetic cloud. Nindos et al. (2003) and Lim et al. (2007) were able to partially reconcile the amount of helicity injected into the corona with the helicity carried away by the CMEs in the ARs they studied. However, the uncertainties of these studies are significant primarily due to the large uncertainties in the calculation of the helicity transported away by CMEs.

Using line-of-sight magnetograms together with the Démoulin and Berger (2003) formula (equation 22), one cannot calculate separately the advection and the shearing terms of equation 20. Furthermore, the validity of the Démoulin and Berger hypothesis has been questioned (see section 3.2). Theoretical studies (e.g. Démoulin et al. 2002a) indicate that on the AR scale transient shearing motions are a rather inefficient way to bring helicity into the corona, compared to the helicity carried by the emergence of a significantly twisted flux tube. However, this is hard to prove observationally. The separate computation of both the shearing and advection terms requires the use of photospheric vector magnetograms. Several methods have been developed towards this goal and contradictory results have been reported (e.g., Kusano et al. 2002; Welsch et al. 2004; Longcope 2004; Georgoulis and LaBonte 2006; Schuck 2008; Zhang et al. 2012; Liu and Schuck 2012). Furthermore, the methods which were developed before 2007 were checked against the same anelastic MHD simulation (Welsch et al. 2007) and produced different results.

On solar cycle time scales, the helicity injected into ARs has an upper limit of 6.6×10^{45} Mx^2 and is an inherently disorganized, impulsive and aperiodic process (Georgoulis et al. 2009). The whole solar-cycle value for the quiet Sun is about 10^{43} Mx^2 (Welsch and Longcope 2003).

4.2 Hemispheric helicity rule

4.2.1 Observations

All helicity proxies discussed in section 3 reveal that solar magnetic fields, at different spatial scales, show primarily negative chirality (i.e. negative helicity sign) in the northern hemisphere while those in the southern hemisphere show primarily positive chirality. This trend is called hemispheric helicity rule and a pictorial summary of it appears in figure 7.

Using vector magnetograph observations of ARs and the α_{best}, α_{av} or current helicity imbalance methods (see section 3.3), it has been established (e.g. Seehafer 1990; Pevtsov et al. 1995, 2001; Abramenko et al. 1997; Bao and Zhang 1998; Bao et al. 2000; Hagino and Sakurai 2004, 2005; Zhang 2006; Hao and Zhang 2011; Liu et al. 2014) that the hemispheric helicity rule is a relatively weak statistical trend satisfied by 60-75% of active regions.

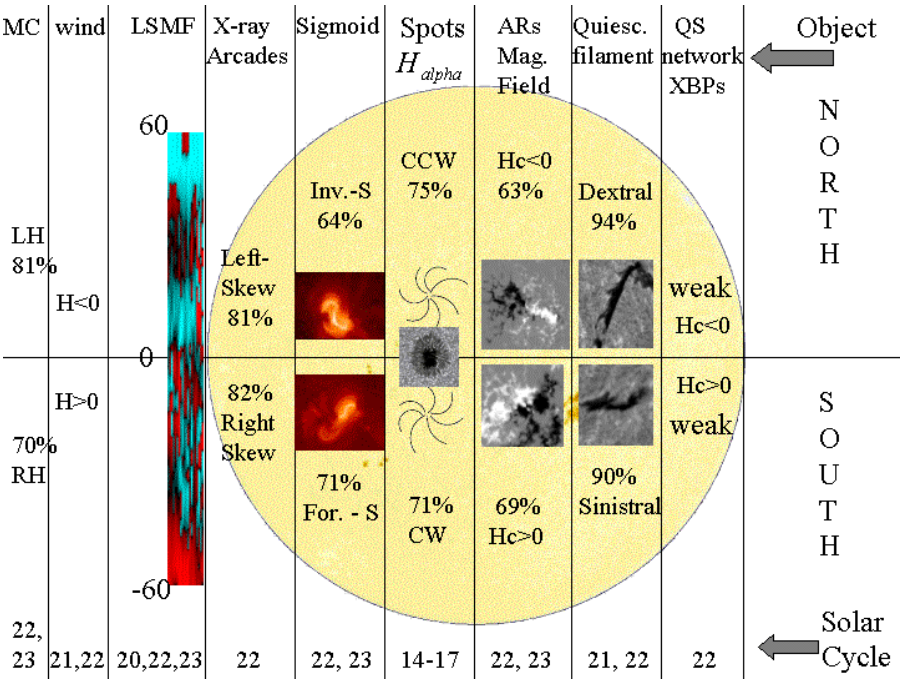

Fig. 7 Pictorial representation of the hemispheric helicity rule. Adopted from Pevtsov (2002).

Soft X-ray sigmoids have also been used as proxies to the chirality of ARs with S (reverse-S) shapes corresponding to positive (negative) chirality. Rust and Kumar (1996); Lim and Chae (2009) determined that the hemispheric rule was obeyed by 80-87% of sigmoids whereas in a larger sample analyzed by Pevtsov and Canfield (1999) the fraction was 64%. We note, however, that potential fields may occasionally show sigmoidal structures (Pevtsov et al. 1997); furthermore the apparent direction of curvature of a three-dimensional sigmoidal structure may depend on projection effects.

The hemispheric helicity rule is also observed in filaments, filament channels, and their overlying coronal arcades (Martin 1998). By visual inspection of the orientation of the "barbs" of both quiescent and active-region filaments Martin (1994); Rust and Martin (1994); Pevtsov et al. (2003); Yeates et al. (2007); Lim and Chae (2009) found that 76-82% of them satisfy the hemispheric helicity rule. However, the corresponding percentage found by Bernasconi et al. (2005) who used an automated detection algorithm was only 68%. Wang (2013) argued that the higher strength of the hemispheric rule in filaments reflects the difficulty in determining the twist in newly emerged ARs, and that the strength of the hemispheric rule in ARs should indeed be similar to that in quiescent filaments.

For the study of the chirality of large-scale solar magnetic fields, proxies of the current helicity were computed from the large-scale vector magnetic fields

which, in turn, were derived from time sequences of longitudinal magnetograms (by tracking the flux as it rotated across the disk and using the changing projection angle to reconstruct its vector components under the assumption that the field did not change over several days, e.g. Pevtsov and Latushko 2000; Wang and Zhang 2010) or even from full-disk vector magnetograms directly (Gosain et al. 2013). Calculations of the helicity injection rate applied on series of synoptic maps derived from longitudinal magnetograms have also been used (Yang and Zhang 2012). Pevtsov and Latushko (2000) did not detect any significant hemispheric chirality asymmetry within $\pm 40^\circ$ of the equator. In their data, however, asymmetry was present at high latitudes where the current helicity was negative (positive) in the northern (southern) hemisphere. The studies by Wang and Zhang (2010); Yang and Zhang (2012); Gosain et al. (2013) found that the hemispheric helicity rule still holds in general, when large-scale fields are considered. Note also that from a large sample of AR vector magnetograms, Zhang (2006) found that weaker fields ($<$500 G) followed the hemispheric rule, but stronger fields had the reverse helicity sign. However, using vector synoptic maps, Gosain et al. (2013) reached exactly the opposite conclusion.

The structures with the smallest spatial scales where the hemispheric helicity rule still holds are quiet Sun network elements (Pevtsov and Longcope 2001, 2007) while the structures with the largest spatial scales include magnetic clouds (e.g. Leamon et al. 2002).

The hemispheric helicity rule does not change from one solar cycle to the other. The study that covered the most time-extended data set was done by Pevtsov et al. (2008) who analyzed data from four different vector magnetograms for 19 years from solar cycles 21, 22, and 23 and found that the hemispheric rule is a weak tendency with significant scatter. However, there are published reports that the rule might change its sign in some periods of a solar cycle. For example, using current helicities Bao et al. (2000) argued that the hemispheric helicity rule was not present at the ascending phase of solar cycle 23. On the other hand, the α_{best} helicity proxy did not show any change in the hemispheric helicity rule for the same period. Hagino and Sakurai (2005) found that the rule is satisfied in the solar maximum phase but may not be satisfied in the solar minimum phase. Hao and Zhang (2011) studied 64 ARs that appeared in the descending phase of solar cycle 23 and the ascending phase of solar cycle 24. The 34 ARs of cycle 24 followed the hemispheric helicity rule, whereas the 30 ARs of cycle 23 did not. However, when combining all ARs as one sample, they followed the hemispheric helicity rule. Zhang et al. (2010) studied AR vector magnetograms from more than 20 years of observations and found that the "wrong" signs disappear at the ends of the butterfly wings as well as at their very beginnings. Furthermore, the large-scale magnetic helicity fluxes computed by Yang and Zhang (2012) showed the same sign in both hemispheres around 2001 and 2005. We note that when we investigate whether or not there is a change of the hemispheric rule with solar cycle we need to take into account how this might be affected by a possible lack of consistency between different magnetograms obtained in the years when the hemispheric

rule is reported to change sign. For example, Pevtsov et al. (2008) argued that due to significant scatter in the data, years with low sunspot activity may show deviations from the rule because the statistical sample is insufficient.

4.2.2 Interpretation

Potential candidates for the origin of the hemispheric helicity rule include solar differential rotation, direct action of the Coriolis force, solar dynamo, and turbulent convection in the upper part of the convection zone.

Wang (2013) showed that the net twist introduced by the Coriolis force on the cross-sectional expansion of each leg of a rising Ω-loop may be substantial if the loop's rise time scale is sufficiently long; he also found that the sense of the twist satisfies the hemispheric rule. But the rule of helicity generation in the hydrodynamic dynamo that is driven by the Coriolis force dictates that the variation of α should be proportional to the sine of solar latitude; this trend is not supported by the observations (Pevtsov et al. 1995).

Differential rotation of the Sun acts over extremely long time scales during which it is unlikely that a single flux tube could survive. But even if we assume so, the maximum possible twist introduced to the tube will be well below observed values (e.g. Longcope et al. 1999; Démoulin et al. 2002b). Furthermore, a fundamental problem with both differential rotation and the Coriolis force is that they are steady mechanisms which lack inherent fluctuations while an intrinsic significant scatter is found in the hemispheric rule.

Choudhuri (2003) has investigated the relation between dynamo theory and the generation of magnetic helicity in flux tubes in the convection zone. He postulated that the toroidal and poloidal fields are generated in two different regions; at the bottom and at the top of the convection zone, respectively. When toroidal flux tubes move upward into the region near the surface where the poloidal field is present, the poloidal field gets wrapped around the flux tube giving rise to helicity. Choudhuri (2003) showed that this process generates helicities with signs that obey the hemispheric rule. Based on this model, computations by Choudhuri et al. (2004) show that at the beginning of a solar cycle the hemispheric rule reverses sign. This is in agreement with some observations (e.g. Bao et al. 2000) but more recent reports (see section 4.2.1) have not confirmed this trend.

The significant scatter exhibited by the hemispheric rule implies that turbulence in the convection zone may play an important role in the generation of the observed chirality trends. Indeed, Longcope et al. (1998) showed that turbulence of the convection zone can introduce to a flux tube helical deformation on small scales (at the mixing length) if the turbulence contains a nonvanishing kinetic helicity. Longcope et al. (1998) called this effect the Σ-effect and showed that these helical deformations will be of the handedness appropriate to explain the scatter observed in the hemispheric helicity rule.

Nandy (2006) provided indirect support in favor of the Σ-effect mechanism. He found that the dispersion in the AR twist distribution is latitude-independent, implying that the amplitude of turbulent fluctuations does not

vary with latitude in the convection zone. His data set also showed that the amplitude and dispersion of twist decreased with increasing magnetic size of active regions, supporting the conclusion that larger flux tubes are less affected by turbulence.

5 Magnetic helicity and the initiation of CMEs

5.1 Helicity as an important agent for CME initiation

Whatever the mechanism that generates helicity on the Sun, it operates continuously. Thus helicity should be removed from the Sun at approximately the same rate as it is created. Accumulation of helicity would make it difficult for solar dynamo to operate – a problem referred to as dynamo quenching (e.g. Brandenburg and Sandin 2004).

CMEs are thought to be the primary agent through which the Sun gets rid of its excess helicity (e.g. Rust 1994; Low 1996; Zhang and Low 2005). The main arguments supporting this idea are: (1) solar magnetic fields obey the hemispheric helicity rule (see section 4.2) which appears not to change from solar cycle to solar cycle. (2) A fraction of AR's helicity is created by the dynamo and then transported into the corona through the photosphere with the emerging magnetic flux. This process would constantly accumulate helicity into the corona because of helicity's property not to be destroyed under reconnection. Furthermore, cancellations of opposite helicity fluxes involves a small fraction of the magnetic flux (e.g. between ARs of opposite helicity sign, either within the same hemisphere or across the equator, Pevtsov 2000). Finally, it is speculated that a small fraction of coronal helicity is cancelled via magnetic reconnection between magnetic fields (ARs and coronal holes) of opposite helicity sign. However, this represents only a small fraction of the accumulated helicity, as the relevant magnetic fluxes are small.

Along the above lines, Low and Zhang (2002) and Zhang and Low (2001, 2003) have developed a unified view of CMEs as the last chain of processes that transfer helicity from the convection zone into the inteplanetary medium. Their theory exploits Taylor's conjecture that the magnetic field will relax towards a LFF field state. A summary of their results is as follows. When new field enters the corona, repeated reconnections between the new and pre-existing field take place. This process simplifies the magnetic topology and the dissipated magnetic energy produces flares. The relaxation proceeds according to Taylor's conjecture and results in the formation of a flux rope which contains a significant fraction of the total helicity of the system. The fate of the flux rope is determined by the efficiency of its confinement by its surrounding anchored field. Flux rope ejection occurs when the magnetic energy it contains is sufficient to drive an outward expansion against the confining field.

In a series of articles, Zhang et al. (2006); Zhang and Flyer (2008); Zhang et al. (2012) studied the theoretical upper limit of helicity that can be stored in various field configurations and its implications for coronal evolution. In the

2006 article they showed that in an open spherical volume like the corona, for a given boundary flux distribution, there is an upper bound on the magnitude of the total helicity of all axisymmetric power-law force-free fields. When the accumulated helicity exceeds this limit, a non-equilibrium situation is reached which mimics the initiation of CMEs. In the 2008 article they found that the helicity upper bound of force-free fields depends on the boundary flux distribution: multipolar photospheric configurations can have a helicity upper bound 10 times smaller than dipolar ones. In the 2012 article they studied the helicity of self-similar axisymmetric force-free fields and found that there may be an upper bound on the total helicity of all bipolar axisymmetric force-free fields. As the helicity increases, the fields open up forming a current sheet surrounded by Parker-spiral-like structures.

Amari et al. (2003a,b) constructed a set of force-free fields having different magnetic flux and helicity contents and used them as initial conditions by applying converging motions or a turbulent diffusion-driven evolution. These processes can trigger eruptive events that may be either confined or global, depending on the value of the initial helicity. Amari et al. (2003b) concluded that helicity cannot be the only parameter controlling the triggering of an ejection, as its value is constant during the diffusion-driven evolution: having a large enough helicity seems a necessary condition for an ejection to occur, but not a sufficient one. Jacobs et al. (2006) performed MHD simulations by shearing an axisymmetric arcade outside a sphere, and found that a twisted flux tube forms and ejects when H/Φ^2 is typically above 0.2–0.3.

5.2 Observational evidence

The physical view presented in section 5.1 has been supported by several observations. Nindos and Andrews (2004) used LFF field extrapolations and the α_{best} method to model the pre-flare coronal field of 78 ARs that produced big flares. Only some 60% of these flares were associated with CMEs. Then from the derived values of α_{best} they computed the corresponding coronal helicities. Their results indicated that in a statistical sense both the pre-flare absolute value of α and the corresponding coronal helicity of the ARs producing CME-associated big flares were larger than the absolute value of α and helicity of those that did not have associated CMEs.

The above results are consistent with the ones reported by LaBonte et al. (2007) who calculated the helicity flux in 48 ARs that produced X-class flares and in 345 non-X-flaring ARs. They found that a necessary condition for the occurrence of an X-class flare is that the peak helicity flux has a magnitude $> 6 \times 10^{36}$ Mx^2 s^{-1}.

Tziotziou et al. (2012) used the method developed by Georgoulis et al. (2012, see section 3.1) to calculate the instantaneous magnetic free energy and helicity from 162 vector magnetograms in total of 42 different ARs. They found a statistically significant, monotonic correlation between the free energy and helicity. This correlation implies that, in addition to helicity, free energy

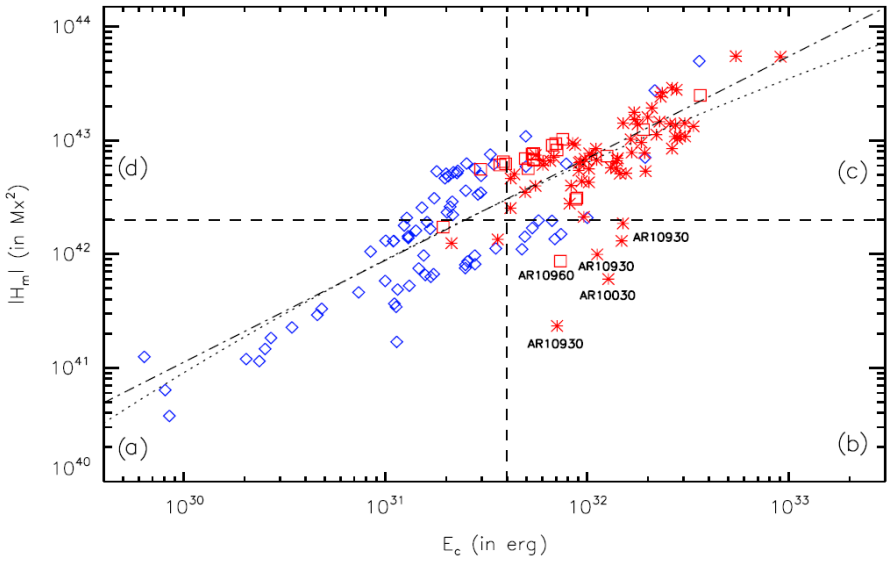

Fig. 8 Free energy-helicity diagram of ARs. Diamonds, squares and asterisks correspond to non-flaring, M- and X-class flaring ARs, respectively. Dashed lines indicate the estimated thresholds for helicity and magnetic free energy above which ARs give major flares. These thresholds divide the diagram into four regions, labeled a, b, c, and d. The dotted and dashed-dotted lines denote the least-squares best fit and the least-squares best logarithmic fit, respectively, between helicity and magnetic free energy (from Tziotziou et al. 2012).

may play a significant role in eruptive phenomena. In their study, the eruptive ARs appeared well segregated from the non-eruptive ones in both free energy and helicity (see figure 8).

In ARs, a primary constraining force that inhibits global eruptions is provided by the overlying background field. Using both line-of-sight and vector magnetograms, Nindos et al. (2012) studied the long-term evolution of the background field in AR11158 that produced three major CMEs. In their calculations they used the decay index of the magnetic field which is a parameter that quantifies how fast the field decreases with height. Their results indicated that the initiation of eruptions did not depend critically on the temporal evolution of the variation of the background field with height. On the other hand, they showed that both the magnetic free energy (computed from NLFF field extrapolations) and the accumulated helicity into the corona (computed from the helicity injection rate) contributed the most to the eruptions by their increase throughout the observations (by factors of more than 5 and more than two orders of magnitude, respectively; see figure 6).

5.3 Other approaches

There are several other approaches to the initiation of CMEs and the role of helicity. Some models suggest that eruptive events can occur without any sig-

nificant helicity accumulations. MacNeice et al. (2004) studied the evolution of helicity under the breakout model (Antiochos et al. 1999). In their simulation, the model was driven by a shear flow that injected both free energy and net helicity into the corona. Their results showed that the helicity shed by the plasmoid ejection was at least 80% of the total originally injected into the system. They interpreted this result as an indication that although CMEs remove the bulk of the coronal helicity, some fraction remains behind. They suggested that some other mechanism (possibly small-scale diffusion) might be responsible for dissipating the rest of the helicity. Furthermore, Kliem et al. (2011) found that simulated flux rope CMEs carried away only a minor part of the initial helicity that was present in the simulation box; most of the helicity remained in the simulation box even after the departure of the CME from there. This result was interpreted as a consequence of the requirement that the current through an expanding loop must decrease if the magnetic energy of the configuration is to decrease as the loop rises, to provide the kinetic energy of the CME.

Phillips et al. (2005) presented simulations of the breakout model where eruption occurs even when no net helicity is injected into the corona. In their simulations the eruption occurs at a fixed magnitude of free energy in the corona, independent of the value of helicity. It would be desirable to check these results against computations of the helicity evolution in observed eruptions that appear to be due to breakout. The MHD simulations by Zuccarello et al. (2009) also showed that the injection of helicity is not a necessary constraint in the initiation of CMEs. However, the absence of significant net helicity accumulation prior to an eruption might result from the accumulation of similar amounts of both positive and negative helicity; in such case the "helicity annihilation" might be at work (Kusano et al. 2003). Indeed, Kusano et al. (2004) presented simulations where the introduction of a reverse helicity was essential for the eruption of a sheared arcade.

The helicity content of a twisted flux rope with a uniform twist across its section and having N number of turns is simply N, when it is measured in units of its flux to the second power. It is convenient to express helicity values in number of end-to-end twist and turns, i.e. in units of the square of the magnetic flux of the active region. For example in an active region with a total magnetic flux and helicity of $\Phi = 5 \times 10^{21}$ Mx and $H = 1.25 \times 10^{43}$ Mx^2, respectively, helicity can be expressed as $N = 0.5\Phi^2$, i.e. the global helicity of the flux rope forming the active region can be characterised as having 0.5 end-to-end turn, equivalent to 1π. In the solar corona twist values are usually low, below $N = 1$, or 2π. However, in the interplanetary medium magnetic clouds are significantly more twisted: values can reach $N = 10$ (Gulisano et al. 2005; Démoulin 2008). The increase in end-to-end twist likely takes place during CME eruption via magnetic reconnection between the erupting flux rope and the sheared arcade field below (Mandrini et al. 2005; Attrill et al. 2006).

Magnetic helicity of a thin flux rope can also be expressed via its twist (T_w) and writhe (W_r, see Section 2.4). Since magnetic helicity is conserved in ideal MHD, twist can be converted into an equal amount of writhe. Such a

conversion takes place during kink instability (e.g. Török and Kliem 2005). The threshold of kink instability is reached at around a twist of 2π. As presently twist cannot be directly measured in the corona, Török et al. (2014) asked the question whether or not the amount of writhing of erupting flux ropes, proxyed by erupting filaments, which is a more directly measurable quantity, could provide quantitative information on the amount of twist in the pre-eruptive magnetic configuration. They carried out MHD simulations of kink instability with a range of internal twists ($3.0 - 10.6\pi$) and found that up to a high initial twist of 7.5π the rope axis invariably develops a one-turn helix, i.e. the amount of twist converted to writhe being about 2π (for an observational example see Williams et al. 2005). Writhing only increased for the highest initial twist values, which are well above twist values usually observed on the Sun. (Although several examples were found by Vršnak et al. (1991) of end-to-end twist of pre-eruption prominences being in the range $3 - 15\pi$, and another example by Romano et al. (2003) of about 10π). Therefore from writhing of erupting filaments one can determine the sign of twist/helicity in the active region (Green et al. 2007), but can only deduce whether or not they are twisted less or more than about 6π.

Moreover, several proposed eruption mechanisms do not explicitly rely on helicity. These models include the tether cutting (e.g. Moore et al. 2001), breakout (Antiochos et al. 1999), magnetic flux cancellation (e.g. van Ballegooijen and Martens 1989). On the other hand, helicity is at the heart of the helical kink instability (e.g. Rust and Kumar 1996; Török and Kliem 2005; Kliem et al. 2012), which has been invoked to explain several eruptive phenomena.

6 Active region tilt

6.1 Introduction of Joy's Law

Sunspots do not form randomly over the solar photosphere, but develop in groups, or active regions. Typically, active regions are elongated in East-West direction. Early observations of magnetic fields indicated that active regions are represented by bipolar patterns, with leading and following sunspots having opposite magnetic polarities. Leading sunspots in opposite hemispheres have opposite polarities: for example, in current cycle 24, leading sunspots of active regions in Northern hemisphere have negative polarity field, while leading spots in southern hemisphere have positive polarity field. In subsequent cycle, these polarities will reverse (leading positive polarity in the Northern hemisphere and negative in the southern hemisphere). Collectively, these patterns, are now known as Hale (or Hale-Nicholson) polarity rule. In both hemispheres, leading sunspots of all groups are situated closer to solar equator then the following sunspots. The average angle between the main axis of the active region and the line of parallel latitude (or equator) is a function of latitude. This dependence of active region tilt on latitude is commonly referred to as

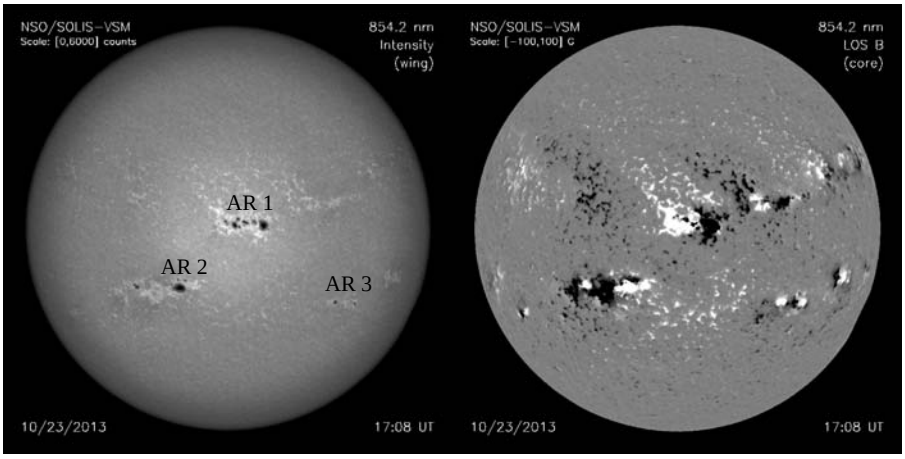

Fig. 9 White light image (a) and corresponding magnetogram (b) showing dark sunspots surrounded by bright plages (left) and the associated magnetic fields (right, white color corresponds to positive and black is negative polarity field). One of the active regions, AR1, provides example, when using white light image alone would allow to correctly identify active region and its tilt. AR2 does not show a well-developed sunspot in its trailing part, and thus, the determination of tilt is less certain. Furthermore, the small spot on the East of AR2 belongs to another bipole, representing its leading part, so AR2 could also be falsely identified as a bipole, giving incorrect tilt angle. In case of AR3, the observer may erroneously classify two close sunspots as an active region, which will result in incorrect tilt. In this case, two sunspots in area marked as AR3 have the same polarity field, and thus, belong to different groups. Data are from the Solar Optical Long-term Investigations of the Sun (SOLIS) system.

Joy's law (term Joy's law was introduced by H. Zirin in 1988; prior to that, the dependency was referred to simply as active regions tilt). Figure 9 shows examples of patterns associated with the Hale polarity rule and Joy's law.

Although active region tilt can be determined from white light images of active regions (figure 9, left), in some cases, the determination of tilt may have a high degree of uncertainty or even errors (e.g., AR2 and AR3, figure 9). Using longitudinal magnetograms alone may also cause a problem for active regions situated far from the central meridian because of apparent polarity reversal due to projection effects. Therefore, the tilt angle is best determined from the analysis of both white light and magnetic field data.

Both Hale's polarity rule and Joy's tilt law were first noted by Hale et al. (1919). However, the significance of trend in tilt angles was not recognized until much later.

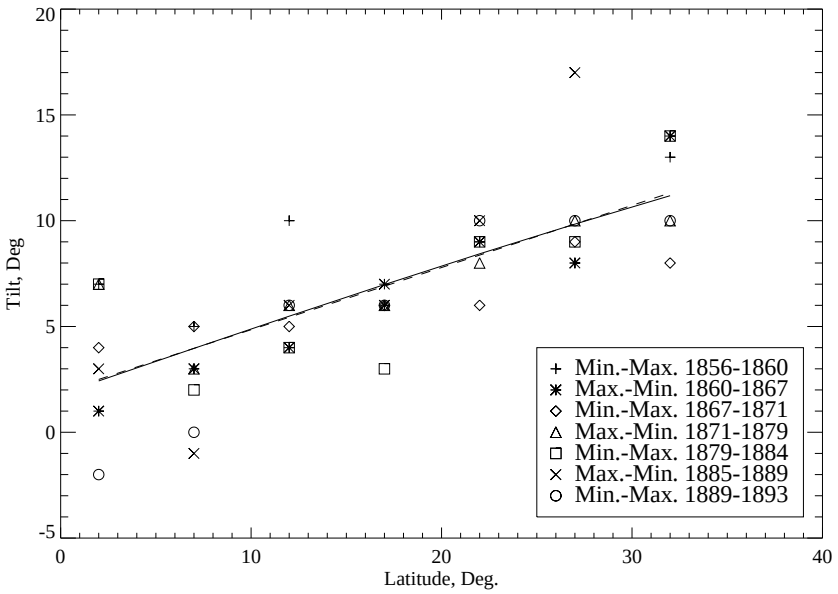

Fig. 10 Joy's measurements of tilt (γ) vs. latitude (φ) averaged over 5 degree latitudinal intervals (0-4°, 5-9°, etc) for rising and declining phases of cycles 10-13 from Hale et al. (1919). Dashed and solid lines show least-square fits by linear functions ($\gamma = (0.29 \pm 0.04) \cdot \varphi + (0.03 \pm 0.01)$) and non-linear ($\gamma = (0.31 \pm 0.04) \sin\varphi + (0.03 \pm 0.01)$) functions, where γ and φ are expressed in units of radians.

6.2 Latitudinal dependence of tilt

Using sunspot drawings by Carrington (1856–1861) and Spörer (1861–1893), Joy (see, Hale et al. 1919) measured tilt of 2633 active regions over three and a half sunspot cycles. He found that the tilt varies with the latitude, and that the tendency is independent of solar cycle. Figure 10 shows Joy's data (see, Table 2 in Hale et al. 1919) and the least-square fit by two functions (done by us). The two fits are nearly indistinguishable from each other. All tilt angles in Figure 10 were determined from white light images only (since magnetogram data was not available prior to 1908) including erroneous tilts determined for anti-Hale and complex polarity spots.

Wang and Sheeley (1989) used line-of-sight magnetograms from the National Solar Observatory (NSO) at Kitt Peak full disk magnetograph to measure tilt of about 2700 bipolar magnetic regions (BMRs) from 1976-1986 (cycle 21). Although, the article provides no coefficients for least-square fit, judging from their figure 6a, the latitudinal dependence is much steeper then in Joy's data. Table 1 provides a summary of fitted functional dependencies to latitudinal variation of tilt angle, $f(\gamma) = A \cdot f(\varphi) + B$, where $f(\gamma)$ and $f(\varphi)$ are functions of tilt and latitude, and A and B are coefficients. For consistency, we converted all fitted coefficients taken from their respected articles to units

of radians. We used data from Hale et al. (1919, Carrington and Spörer, C&S sunspot drawings) and Brunner (1930, Zurich sunspot measurements) to compute the functional approximates, which are shown in the Table 1 with the reference to our present article.

Three different functional dependencies used in these previous studies return very similar results. The first group (γ vs. φ) shows very consistent fits, with the exception of Zurich and CSA (Russian) datasets, for which the tilt is notably higher. We do not have an explanation for this inconsistency, but we speculate that this could be related to the sampling of active regions for two data sets. In both cases, the selection was done by the observer, and thus, it could be that the size of selected regions played a role. We note that in comparison with Mount Wilson (MWO) and Kodaikanal (KK) observatories, CSA data set show significantly smaller scatter in tilt angles (Ivanov 2012), which indirectly supports the idea that the determination of active regions in this data set was emphasizing larger regions.

In the second group (γ vs. $\sin\varphi$) fits to the Carrington and Spörer (C&S) and to MWO data are in agreement with the results for the first group. Latitudinal dependence of tilt derived from longitudinal magnetograms from SOHO/MDI (Stenflo and Kosovichev 2012) is steeper and it is in a better agreement with fit to Brunner (1930) data.

In the third group ($\sin\gamma$ vs. $\sin\varphi$), fit to C&S data is in agreement with the first and second groups, but fits to NSO/KP and Zurich data are much steeper. Overall, it appears that fitting the orientation of bipolar magnetic regions (BMRs) returns higher tilt as compared with the data based on white light images and sunspot drawings. The latter may be the effect of the difference in evolutionary state of active regions covered by the white-light and magnetic datasets of active region tilt angles. White-light signatures active regions (sunspots) have shorter life span than that of the magnetic signatures of BMRs distinguishable from background field. Therefore the difference between tilt angles obtained from white-light and magnetic datasets may rather result from the dominance of active regions in their decay phase in the magnetic data sets, while the white-light (sunspot) data is dominated by relatively young active regions.

We also note that more than half of the linear fits shown in Table 1 return a non-zero intersect point (corresponding to about 1-2 degrees) which suggests that even at the equator the active regions have a slight non-zero tilt. Many fits are forced through the origin on the assumption that active regions have a zero tilt angle at the equator. This is done because it is assumed that the Coriolis force is the only contribution to the tilt angle value. Since all the physical processes that contribute to the tilt angle are not yet understood, it is best to fit the data and not assume that tilt angles are zero at the equator. As an example, NOAA active region 11987 was a Northern hemispheric polarity group with the leader at -2 degrees southern latitude and the follower spot on or slightly above the equator. This group basically formed a bridge across the equator and maintained a healthy tilt angle of $\approx$15–18 degrees from when it was visible on 22 Feb 2014 until the follower spot broke apart on 27 Feb 2014.

This is just one example of active regions near the equator not having a zero tilt angle. More studies should be done on the tilt angles of active regions that emerge within several degrees of the equator as their existence contradicts the conventional wisdom of Coriolis force imparting the largest portion of the tilt.

While in most cases tilt vs. latitude dependence is assumed to be monotonic with latitude, some data indicate a possible presence of maximum in tilt angles in mid-latitudes. The maximum can be seen in MWO, KK and CSA data (Sivaraman et al. 1999; Ivanov 2012). Due to reduced size of statistical sample for high latitudes, standard deviations of the means are also large, and thus, this apparent decrease may be statistically insignificant. Still, this may need additional studies to confirm (or disprove) the presence of a peak in tilt angles in mid-latitudes.

Table 1 Summary of latitudinal functional dependence

Tilt function	A	Latitude function	B, radian	Type	Dataset	Years	Reference
γ	0.29±0.04	φ	0.03±0.01	WL[1]	C&S[3]	1856–1893	Pevtsov et al. (2014)
γ	0.26±0.05	φ		WL	MWO[7]	1917–1985	Dasi-Espuig et al. (2010)
γ	0.28±0.06	φ		WL	KK[5]	1906–1987	Dasi-Espuig et al. (2010)
γ	0.26±0.02	φ		WL	MWO	1917–1985	Ivanov (2012)
γ	0.28±0.03	φ		WL	KK	1906–1987	Ivanov (2012)
γ	0.38±0.03	φ		WL	CSA[4]	1948–1991	Ivanov (2012)
γ	0.55±0.03	φ	-0.02±0.01	WL	Zurich[9]	1894–1928	Pevtsov et al. (2014)
γ	0.50±0.20	φ	-0.02±0.01	MG	MWO & MDI[6]	1976–2010	Li and Ulrich (2012)
γ	0.31±0.04	$\sin\varphi$	0.03±0.01	WL	C&S	1856–1893	Pevtsov et al. (2014)
γ	0.56±0.01	$\sin\varphi$		MG[2]	MDI	1995–2011	Stenflo and Kosovichev (2012)
γ	0.27±0.01	$\sin\varphi$		WL	MWO	1917–1985	Fisher et al. (1995)
γ	0.58±0.04	$\sin\varphi$	-0.02±0.01	WL	Zurich	1894–1928	Pevtsov et al. (2014)
$\sin\gamma$	0.50	$\sin\varphi$		WL	Zurich	1894–1928	Leighton (1969)
$\sin\gamma$	0.57±0.04	$\sin\varphi$	-0.02±0.01	WL	Zurich	1894–1928	Pevtsov et al. (2014)
$\sin\gamma$	0.31±0.04	$\sin\varphi$	0.03±0.01	WL	C&S	1856-1893	Pevtsov et al. (2014)
$\sin\gamma$	0.48	$\sin\varphi$	0.03	MG	NSO/KP[8]	1976–1986	Wang and Sheeley (1991)

[1] WL – white light filtergrams and/or drawings
[2] MG – line-of-sight magnetograms
[3] C&S – Carrington and Spörer datasets
[4] CSA – the Pulkovo observatory's "Catalogue of Solar Activity"
[5] KK – Kodaikanal observatory
[6] MDI – Michalson Doppler Imager
[7] MWO – Mount Wilson Observatory
[8] NSO/KP – National Solar Observatory at Kitt Peak
[9] Zurich – sunspot drawings

6.3 Non-Hale polarity regions and δ-spots as highly tilted bipoles

Active regions' tilt is a weak tendency with significant scatter (for example, see Fisher et al. 1995). In contrast, Hale polarity law is a strong dependence. For example, in MWO data set from 1913-1917, annual fraction of non-hale polarity regions vary between 1.4–6.3% with average of about 3.7% (Hale et al. 1919). More recent data from SOHO/MDI reveal similar fraction of about 4% (Stenflo and Kosovichev 2012). Li and Ulrich (2012) found a larger fraction between 6.5% and 9.1% for cycles 21–23. Non-Hale polarity regions could be interpreted as highly tilted regions, whose main axis is rotated by about 180°. In support of that interpretation, Pevtsov and Longcope (1998) described a linked appearance of Hale and non-Hale polarity regions. Two regions shared a common polarity, which first appeared as the leading polarity for Hale polarity BMR and on the sequential solar rotation, it was the following polarity of a non-Hale active region. López Fuentes et al. (2000) described evolution of anti-Hale bipolar active region, in which over four solar rotations one magnetic polarity was gradually moving around the other opposite polarity flux; with the corresponding BMR changing its orientation from Hale to non-Hale polarity. Based on the observation that the non-Hale polarity regions develop at any phase of sunspot cycle, Stenflo and Kosovichev (2012) speculated about the presence of two toroidal fluxes with opposite orientation in the convection zone.

δ-spots are another type of irregular sunspots, which show a significant deviation from Joy's tilt and Hale polarity rules. A δ-spot consists of two (or multiple) umbrae with the opposite polarity magnetic field within a single

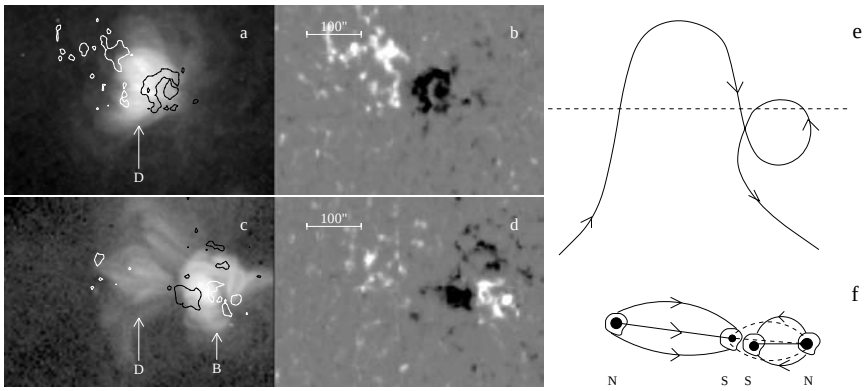

Fig. 11 Left: NSO/Kitt Peak line-of-sight magnetogram (b and d) and soft X-ray Yohkoh image (a and c) showing the overall structure of NOAA AR 7918 and AR 7926. White indicates positive (N) flux and black negative (S). The contours overlaying the coronal image correspond to ±100 G of the line-of-sight magnetic field. Arrows indicate two different sets of the loops. (a) NOAA 7918, 1995 October 28, 18:30:39 UT; (b) NOAA 7918, 1995 October 28, 17:54:37 UT; (c) NOAA 7926, 1995 November 21, 16:34:35 UT; (d) NOAA 7926, 1995 November 21, 16:47:50 UT. Right: Model of Ω-loop with stitch. Arrows show direction of the magnetic field in the loop. (e) Side view of the loop. The dashed line indicates the photosphere. (f) Top view of the loop schematically showing sunspots at the places where the Ω-loop crosses the photosphere. Full lines with arrows show magnetic field lines above the photosphere projected onto the horizontal plane. Dashed lines indicate subsurface parts of field lines. Based on figures 2 and 8 from Pevtsov and Longcope (1998).

penumbra. Line connecting opposite polarity umbrae is usually highly tilted relative to solar equator. Based on change in orientation of δ-spots during their evolution, this type of sunspot groups has been interpreted in the framework of the emergence of highly kinked flux tubes. δ-spots show a well-defined pattern of electric currents with current flowing upward in one umbra and the downward in the other umbra (Pevtsov 2003). This pattern supports the notion that these sunspots are associated with single (but highly twisted) magnetic flux tubes.

6.4 Changes in the tilt angle during the lifetime and evolution of active regions

Observations suggest that active regions do not emerge with the "right" tilt, but the tilt develops rapidly during the first few days as the region emerges through the photosphere (for example, see Pevtsov et al. 2003a). As active regions decay, their tilt relaxes to a mean tilt for a given latitude (Howard 1996; Kosovichev and Stenflo 2008). The latter was interpreted as an indication that the tilt is not the result of the Coriolis force action. According to this argument, since the Coriolis force vanishes once the emergence stopped, the tilt should relax to East-West direction. Kosovichev and Stenflo (2008) argued that the relaxation of tilt to a mean (non-zero) value indicates that the tilt represents

the orientation of toroidal field in the convection zone. However, Longcope and Welsch (2000) suggested that the evolution of tilt and twist may depend on how rapidly the active region emerges through the photosphere. This theoretical prediction was later confirmed by the observations (Pevtsov et al. 2003a). Subsequently, one can argue that tilt may represent writhe component of helicity in the magnetic flux tubes forming active regions. Then, the relaxation of active regions to a mean (non-zero) tilt may be related to helicity content of active regions for a given latitude (e.g. Canfield and Pevtsov 1998).

The presence of a global twist in emerging flux tube can modify the tilt angle of the emerging bipole when it is measured in magnetic data. Luoni et al. (2011) show that while the flux rope is breaking through the photosphere, a characteristic elongated asymmetric polarity pattern, dubbed magnetic tongues or tails, develops in the line-of-sight magnetograms owing to the presence of azimuthal field components. The pattern is dependent on the sign of the global twist and thus provides a simple proxy for it (López Fuentes et al. 2000; Luoni et al. 2011). In magnetograms magnetic tongues or tails may mask the true tilt angle of the bipole, since the tongue pattern resulting from e.g. negative/positive global twist on the northern/southern hemisphere shifts the centre of gravity of magnetic polarities introducing an angle which is opposite to that of Joy's law (cf. Figure 12). Therefore the tilt angle of those bipoles, which obey the hemispheric helicity rule, may be cancelled or reduced (while the tilt angle of those bipoles, which disobey the hemispheric helicity rule are enhanced) by this effect during the emergence process and the bipole will only assume the Coriolis-induced tilt when the entire flux rope has crossed the photosphere and the tongues/tails have retracted.

6.5 Variations with cycle, size of active region, magnetic flux

Several studies searched for a correlation between the active region tilt and the amplitude of solar cycle. While the studies showed some indication of such dependency, overall the results are still not well-understood. Dasi-Espuig et al. (2010) found a strong negative correlation between the strength of solar cycle and the area-weighted mean tilt value normalized by latitude. Both MWO and KK data exhibited equally strong correlation. This is a very interesting idea that a strong cycle would produce bipolar active regions with lower average tilt-angles and therefore a lower polar flux amplitude (and vice versa for a weak cycle producing more highly tilted regions), as such creating a mechanism that is self-regulating the cycle amplitude since many dynamo models consider the polar flux amplitude to be the seed field by which the strength of the solar cycle is set. Later, however, Ivanov (2012) and McClintock and Norton (2013) were not able to reproduce the exact dependency found in Dasi-Espuig et al. (2010) for MWO data. Dasi-Espuig et al. (2013) revised their results in agreement with Ivanov (2012) and McClintock and Norton (2013) findings. Dependency between the amplitude of solar cycle and the tilt angle found by McClintock and Norton (2013) is in a general agreement with

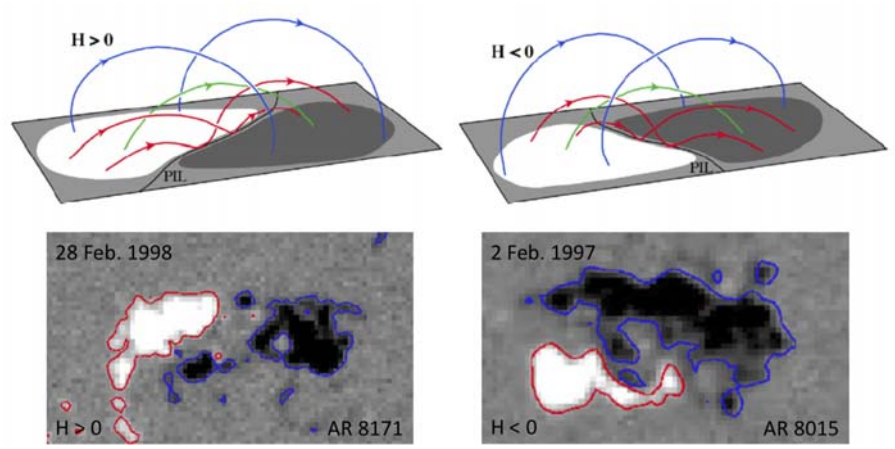

Fig. 12 Top: Sketches of magnetic "tongue" patterns in longitudinal magnetograms with (left) positive and (right) negative global twist in the emerging flux rope, which develop owing to the presence of the transverse magnetic field component. Representative field lines of the enveloping arcade and internal (dipped) field lines are also shown, so is the polarity inversion line (PIL). Bottom: Two examples of magnetic tongue pattern during the emergence of AR 8171 (left) and AR 8015 (right) corresponding to the helicity sign as the sketches above them. Both the sketches and the SOHO/MDI observations were adapted from Luoni et al. (2011)
.

Ivanov (2012) and the revised findings by Dasi-Espuig et al. (2010). However, the McClintock and Norton (2013) analysis separated the data by hemisphere and found that the correlation of cycle strength and area-weighted mean tilt angle normalized by latitude only held for the Southern hemisphere for cycles 15-21. The dependence was insignificant for the Northern hemisphere data. One can question the validity of the proposed dependency if both hemispheres do not exhibit it. Also, the negative correlation between the amplitude of solar cycle and the normalized tilt angle for MWO data appears primarily due to the data point corresponding to solar cycle 19. If this data point is excluded, MWO data show no correlation with solar cycle.

Action of the Coriolis force on emerging flux tube depends on several parameters including total magnetic flux and the field strength at the axis of flux tube. Fan et al. (1994) predicted that the tilt angle γ will depend on total magnetic flux Φ, maximum field strength B_0 at the bottom of the convection zone, and latitude φ as following: $\gamma \propto \Phi^{0.25} \cdot B_0^{-1.25} \cdot \sin\varphi$. Since both the maximum field strength and the magnetic flux in sunspots correlate with their size (e.g., Tlatov and Pevtsov 2014), one would also expect to see a correlation between tilt angle and active region area. Study of tilt properties of 27,701 active regions from MWO data set (Fisher et al. 1995) concluded that the functional dependency of tilt on foot-point separation and sine of latitude appears to be in agreement with the predictions of Fan et al. (1994) model. They also estimated the field strength in flux tubes at the bottom of the convection zone B_0 = 20-30 kG.

It has been noted (Howard 1991; Sivaraman et al. 1999) that it is large active regions that follow the Joy's law most closely. On the other hand, Ivanov (2012) found that CSA data set deviates from that dependency. Tlatov et al. (2010) analyzed the orientation of magnetic bipoles over three solar cycles 21-23 using NSO/KP and SOHO/MDI longitudinal magnetograms. The bipoles were classified by their area as quiet Sun bipoles (QSBs, area, A, smaller than 50 millionth of solar hemisphere, MSH), ephemeral regions (ERs, 100 MSH $\leq$A$<$ 500 MSH), and regular active regions (ARs, A$\geq$ 500 MSH). QSBs were found to exhibit a random orientation independent of latitude, which suggests their formation via a random encounter of their foot-points. ERs and ARs followed the Joy's law in their orientation, with ERs showing larger scatter in their tilt angles relative to the mean. Scatter in tilt angles is usually contributed to convective buffeting, or interaction of magnetic flux tube with turbulent convection as it rises through the convection zone. Longcope and Fisher (1996) found that the amplitude of fluctuations in tilt angles should be inversely proportional to foot-point separation, and thus, smaller bipoles should exhibit much larger fluctuations in their tilts. The latter supports Tlatov et al. (2010) findings for ERs scatter in their orientation. Tlatov et al. (2010) also found that around the maximum of previous cycle, high latitude ERs had their polarity orientation (Hale polarity rule) corresponding to a subsequent solar cycle. The latter was interpreted as the indication of extended solar cycle (Wilson et al. 1988).

Time variation of active region tilt within solar cycle follows the properties of active regions. As new cycle starts, the active regions appear at high latitudes with their tilt and polarity orientation corresponding to this cycle. As cycle progresses, the latitude of active region emergence moves towards the equator. In that respect, the time variation of tilt angles is more reminiscent to the butterfly diagram of sunspots, and is dissimilar to a sunspot number plot.

A possible difference in Joy's law between northern and southern hemispheres was noted by several researchers (Dasi-Espuig et al. 2010; McClintock and Norton 2013; Li and Ulrich 2012). Based on the analysis of the tilt angle data separated by hemisphere, McClintock and Norton (2013) recommend a revision of Joy's law toward a weaker dependence on latitude (slope of 0.13–0.26) and without forcing the tilt to zero at the equator. They determined that the hemispheric mean tilt value of active regions varies with each solar cycle, although the noise from a stochastic process dominates and does not allow for a determination of the slope of Joy's law on an 11-year time-scale. The hemispheric difference in mean tilt angles, $1.1^\circ \pm 0.27$, over Cycles 16 to 21 was significant to a three-σ level, with average tilt angles in the northern and southern hemispheres of $4.7^\circ \pm 0.26$ and $3.6^\circ \pm 0.27$ respectively.

When analyzing the active regions of a single hemisphere in a single solar cycle, Joy's law only appears weakly (see figure 13, McClintock and Norton, 2013). A linear function is a poor fit to the data in most cases. The linear correlation coefficients range from r = 0.18 (cycle 17 North, cycle 19 South) to r = 0.86 (cycle 20 North). The large amount of scatter and high noise

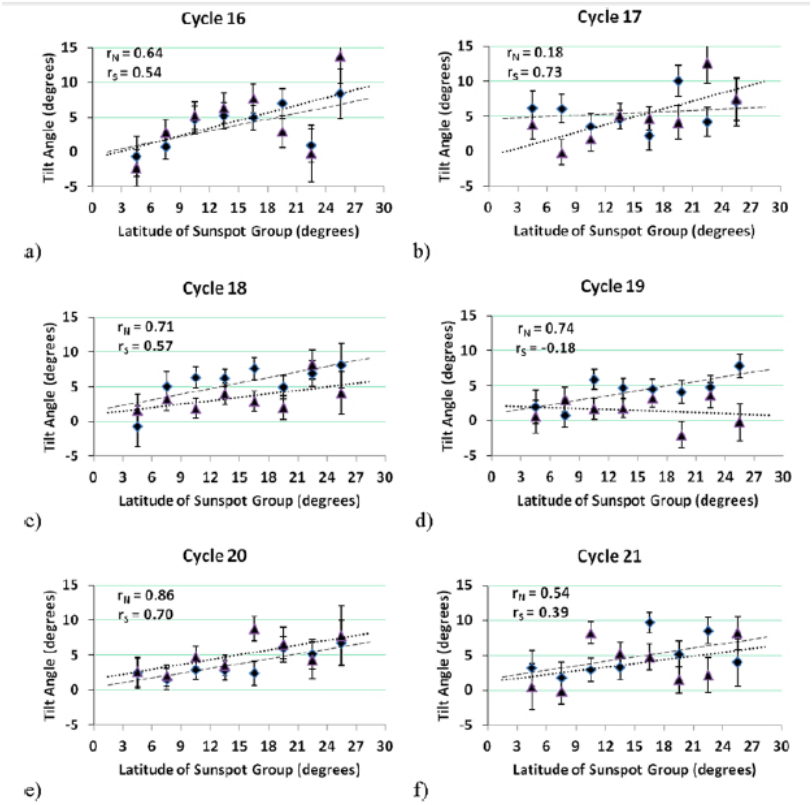

Fig. 13 Tilt angle of bipolar active regions as a function of latitude for the North (diamond) and South (triangle) hemispheres for cycles 16 21 are shown in panels (a)-(f), respectively. Data were binned in 3° of latitude. Standard errors of the mean are overplotted as error bars. Linear fits to Northern (dash) and Southern (dot) hemisphere data are shown with linear correlation coefficients [r_N, r_S] included in the legends. The fits were not forced through the origin. Courtesy McClintock and Norton (2013).

apparent in Joy's law is interesting, because it indicates that a stochastic process is competing with the mechanism that determines the tilt angles. The stochastic process dominating Joy's law on the short time scale is considered to be turbulent convection imparting random tilt angles to the rising flux tubes (Fisher, Fan, and Howard, 1995; Weber, Fan, and Miesch, 2012). Dasi-Espuig et al. (2010) also state that "no clear difference could be determined between the slopes of Joy's law from cycle to cycle," as can be seen in figure 13; therefore, we use the mean tilt value from each hemisphere for each cycle to analyze the hemispheric differences.

McClintock and Norton (2013) argue it is possible that the recovery of a mean bipolar region tilt angle and scatter for a given solar cycle can be used as a diagnostic for that cycle, i.e. the strength of the cycle as indicated by Dasi-Espuig et al. (2010) or the geometry/orientation of the toroidal fields

from which the flux ropes begin their initial rise (Babcock, 1961; Norton and Gilman, 2004).

They also point out why specific bins in the Southern hemisphere in Figure 13 showed such different behavior from the other bins. For example, late in all solar cycles (except cycle 20) aberrant activity occurred at the 18–21° latitudes. In particular, the Southern hemisphere during cycle 19 is very disorganized, with the high-latitude bins of 18–21° (304 regions, 24%) and 24–27° (150 regions, 12%) having negative mean tilt values, meaning that these bipolar regions have a following spot closer to the Equator than the leading spot. It would be interesting to study this in more detail and better understand the conditions favorable for aberrant configurations, i.e. anti-Hale and negative tilt angles, to occur.

McClintock and Norton (2013) found that cycles 18 and 19, as well as the data averaged over all cycles 16–21, show that the mean tilt angles differ significantly between the hemispheres. For example, they found an average value of mean tilt for cycle 18 to be 5.7±0.61 in the Northern hemisphere while the mean tilt value was 2.9±0.6 in the Southern hemisphere. The different hemispheric and cycle mean tilts, and different slopes of Joy's law, warrant closer scrutiny.

6.6 Tilt and helicity

The action of an external force (e.g., Coriolis force) that distorts the shape of a flux tube will introduce writhe, Wr and twist components of helicity, Tw into the flux tube. If initially the flux tube had zero helicity $H = Tw + Wr = 0$, the twist and writhe will have an opposite sign ($sign(Tw) = -sign(Wr)$). If, on the other hand, the flux tube had a non-zero (say, positive) helicity, and the writhe developed as the result of kink-instability, then part of the internal twist was traded for writhe, and the two should have the same sign ($0 < H = Tw + Wr; sign(Tw) = sign(Wr)$). These arguments were first put forward by Canfield and Pevtsov (1998) and Pevtsov and Canfield (1999), who studied the correlation between tilt and helicity density proxy of 99 ARs observed by the Haleakala Stokes Polarimeter (HSP). The helicity proxy was represented by average α coefficient in force-free field fit to the observed magnetic field. A weak negative correlation between sign of tilt and sign of α was found for active regions that significantly deviate from Joy's law. This negative correlation is contrary to the expected dependence introduced by the action of the Coriolis force on a rising flux tube. Hence, Pevtsov and Canfield (1999) concluded that at least in some cases, the tilt of active regions could be the result of kink-instability of active regions with non-zero helicity. (In this study, the writhe was defined as being positive in counter-clockwise direction from E-W direction. This definition is similar to a regular Cartesian coordinate system. On the other had, traditionally, active region's tilt is defined as positive angle in clockwise direction from W-E direction. Thus, positive tilt will correspond to negative writhe).

On the other hand, Tian et al. (2001) compared the sign of tilt and twist and found a positive correlation. They concluded that twist in active region magnetic fields is the result of the Coriolis force acting on the apex of emerging-loops, which introduces both twist and writhe in originally untwisted magnetic fields. In a later study, Tian and Liu (2003) found evidence of kink-instability in their study of tilt–twist relation for 86 flare-productive active regions. Study of tilt–twist relation for 22 active regions, López Fuentes et al. (2003) found both twist and writhe with the same sign (supporting kinking) and with opposite signs (Coriolis force action) in about 35% and 41% of cases, respectively. Holder et al. (2004) conducted an extensive study of tilt–twist (helicity) relation for 356 active regions. Helicity proxy α coefficient was computed using vector magnetograms from the Haleakala Stokes Polarimeter (HSP) and tilt angles were taken from MWO data set. They found weak (but statistically significant) negative correlation (opposite sign of tilt and twist) supporting the the kink-instability scenario. The correlation was even stronger for active regions deviating from the general tendency for the hemispheric helicity rule, which further supports the kink-instability as the origin of tilt for these regions. Non-Hale polarity regions were found having a positive correlation (same sign of tilt and twist). Again, the latter supports the kink-instability scenario if non-Hale regions are interpreted as bipolar structures tilted in excess of 90 degrees relative to direction parallel to equator. For active regions that follow Joy's tilt law, Holder et al. (2004) found no twist-tilt dependence. They also concluded that the scatter in tilt angles and the dispersion in twist are uncorrelated with each other. Both of these results are in agreement with the effects of convective buffeting of initially untwisted and unwrithed flux tubes, or Σ-effect (Longcope et al. 1998).

Liu et al. (2014) used the relation between tilt and writhe in their study of the strength of hemispheric helicity rule. Observations of 151 active regions from Helioseismic and Magnetic Imager (HMI) were used to derive both twist and writhe. The data showed both the hemispheric helicity rule and the Joy's law. However, the hemispheric helicity rule was found to be significantly stronger for a sub-group of active regions with the same sign of twist and writhe. Liu et al. (2014) concluded that either the flux tubes do not have a hemispheric preference for twist prior to their emergence from the base of the convection zone, or that the initial twist is weak.

6.7 Importance of tilt for solar dynamo

In flux-transport models of solar dynamo (Wang and Sheeley 1991), the magnetic field of following polarity active regions is transported to solar poles, where it interacts with the existing polar field leading to polar field reversal. The polar field may also establish the strength of the next solar cycle (Upton and Hathaway 2014). In this process, tilt of active regions may play important role by either facilitating the creation of polar field (by placing following polarities higher in latitudes via larger tilt) or eroding it. In periods of high

activity active regions are more closely packed, which increases the cancellation rate, including that of across the equator. With increasing tilt angles of active regions opposite polarities of neighboring active regions are more separated in latitude, which decreases inter-active region cancellations. However, cross-equatorial cancellation of the preceding polarities are enhanced.

This will allow more following-polarity flux to be transported to the poles. This was investigated in a parameter study by Baumann et al. (2004) whose model predicted a strong dependency between tilt angle (normalized to latitude of emerging bipole) and the strength of polar magnetic field. This model simulations catalysed search for correlation between mean tilt angle and the strength of sunspot cycle. So far, no conclusive correlation was found (see, Section 6.5). Even if present, the correlation between tilt angle and the strength of solar cycle can be masked by several factors. For example, the strength of polar field from previous cycle may negate the effect of higher tilt angle of active regions from the present cycle. Even though with higher tilts, the magnetic flux of trailing polarity will be transported to the poles in a more efficient manner, it would have to cancel out stronger polar flux. Such effects would need to be taken into consideration in future numerical modelling. Petrie (2012) found in cycle 23 the net poloidal contribution of active regions effectively disappeared in 2004, thereby lowering the polar field strengths significantly as the Sun headed towards the minimum and the beginning of cycle 24. From his analysis he could not determine whether the reduction in net poloidal field was due to a lowering of average tilt angles of active regions or another cause. He notes, however, that there was a notable N-S hemispheric asymmetry present from 2004 and that faster-than-average meridional flows at active latitudes (another mechanism that could produce weak polar fields) were not detected.

6.8 Interpretation of Joy's law

Active region tilt has been interpreted in the framework of three different main underlying causes: toroidal field orientation, action of Coriolis force, and more recently, as signature of kink-instability.

Tilt as a signature of toroidal flux orientation. In the Babcock-Leighton model, at the beginning of cycle, the magnetic field is mostly poloidal (oriented in North-South direction parallel to solar meridian). As the solar equator rotates faster then higher latitudes, the differential rotation action gradually changes the orientation of magnetic field to be more aligned with latitudinal circles. When portion of subphotospheric toroidal flux tube erupts through the photosphere, it forms an active region, whose tilt may reflect a general orientation of the toroidal flux tube (Babcock 1961). Some researchers (e.g., Kosovichev and Stenflo 2008) argued that since the tilt of active regions after the complete emergence does not relax to East-West direction, the tilt must represent the orientation of toroidal field in the convection zone.

To evaluate the validity of this mechanism, we consider a very simplified model, in which two footprints of a flux tube are separated by 2 degrees in latitude and the orientation of the footpoints is that one is northward of the other (in other words, a N-S orientation). Note that we are not discussing the wreath of flux in the interior, but more a cartoon of a thin flux tube. If we assume that the tilt angle (or geometry of the footpoints) is determined only by the difference in rotation rates (differential rotation) for these two latitudes, then we can easily calculate how long it would take to turn a N-S flux tube into an E-W flux tube. This is a simplified example but is worth considering. Figure 14 shows the resulting tilt angles for different latitudes after 1, 5, and 10 solar rotations. After just five solar rations, the toroidal flux tube will be oriented at about 10 degrees relative to the equator, and after ten rotations, the tilt will be less than 5 degrees. Thus, in just a few years after the beginning of solar cycle, the toroidal flux tube should become oriented nearly parallel to solar equator over all latitudes of active region formation. In low latitudes, however, the tilt will remain higher in amplitude as compared with mid-latitudes, opposite to the trend observed. This is one argument against a tilted toroidal flux playing a significant role in orientation (tilt) of active regions at the photosphere. However, this does not take into account that the flux wreath may have an E-W orientation in general, but that individual tubes within the wreath may have a tilt or be more complexly oriented than the larger structure.

The idea that active region tilt may reflect the orientation of subphotospheric toroidal field was further explored by Norton and Gilman (2005) in respect to possible tipping and warping instabilities that may develop in a rotating ring-like magnetic flux tube due to an instability of differential rotation and concentrated magnetic fields. Development of these modes was carried out by Cally et al. (2003), Gilman and Fox (1997) and Gilman and Dikpati (2000) who found that narrow toroidal bands tip about their axis ($m = 1$) if they are ≈100kG while toroidal bands of lesser field strengths may deform or warp ($m > 1$). A toroidal field tipped with respect to the equator would increase the scatter of the mean tilt angle, but not the average value of tilt angle. Norton and Gilman (2005) analyzed extensive data from longitudinal magnetograms from NSO/KP and SOHO/MDI and found the presence of tipping and warping instabilities from the location of active regions, but they did not examine the tilt angles. Note that this model and corresponding analysis is examining the non-axisymmetric nature of the solar dynamo. This is a further complexity in the model and analysis - not only are the hemispheres thought to progress slightly differently during the solar cycle, but the signatures are not averaged over all longitudes. McClintock and Norton (2013) searched for evidence of the tilt and warp (deformation) of the toroidal band from the active region tilt angle data. They found no significant signal in average tilt angle values or tilt angle scatter as a function of longitude. However, this does not prove that the geometry of the toroidal band does not influence the tilt angle, or that the toroidal band in the interior is axisymmetric, only that the variation of tilt

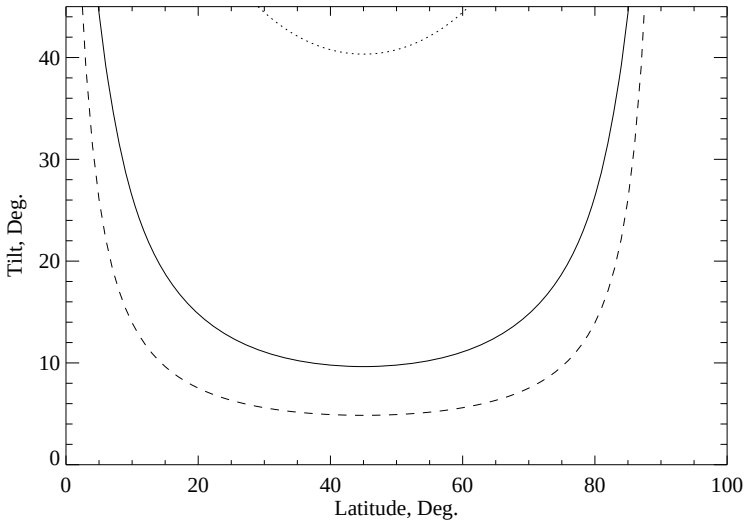

Fig. 14 We assume a simple flux tube were oriented in the N-S direction, horizontal to the solar surface, with the footpoints separated by two degrees of latitude, this plot shows the orientation of the flux tube from the effect of differential rotation after one (dotted), five (solid) and ten (dashed line) solar rotations. This plot is a simplification but is intended to show how quickly flux in the interior becomes purely toroidal and would not maintain a significant tilted geometry unless other factors were considered.

angles as a function of longitude can not be distinguished from the noise in this data.

Tilt as the result of Coriolis force action. The role of the Coriolis force in formation of active region tilt was mentioned by Babcock (1961) and Schmidt (1968). Wang and Sheeley (1991) proposed that as the magnetic flux tube rises through the convection zone and expands, the Coriolis force distorts the apex of the tube tilting it in the way it can explain Joy's law. The scenario was further developed in the framework of 3D thin flux tube model (D'Silva and Choudhuri 1993; Schüssler et al. 1994; Fan et al. 1994). The high scatter observed in tilt angles is generally thought to be caused by the turbulent nature of flow in the convection zone imparting a large variation into the tilt angle values. Later model developments were very successful in reproducing many observational properties of active regions including their tilt, asymmetry between leading and following polarity sunspots in compactness and inclination of magnetic field relative to vertical direction, and large scatter in tilt angles (Weber et al. 2011). By fitting the model predictions with the observations, field strength of toroidal flux is estimated at 40-50 kG at the bottom of the convection zone. The effect of the Coriolis force on active region tilt depends on total rise time of flux tube through the convection zone, which in turn depends on magnetic flux. By varying the magnetic flux, Weber et al.

(2013) were able to explain some differences in tilt-latitude tendencies found by different studies. They argued, for example, that since magnetograms enable selecting structures with weaker magnetic fields, they may show steeper tilt vs. latitude trends as compared with white light images, which are more likely to select solar features with stronger magnetic flux. On the other hand, taking into account the scatter in tilts derived from model calculations, Weber et al. (2013) did not find a strong dependence of tilt on field strength. These later simulations also found about 6.9% of emerging bipoles having non-Hale polarity orientation, which is in a very good agreement with the observations. One of the most interesting aspects of the work done by Weber et al. (2013) is that the simulations of the rise of a thin flux tube in a turbulent, convecting, rotating shell enables an estimation of the expected standard deviations of the tilt angles for a given combination of toroidal field strength in the tachocline and flux in the rising tube.

Tilt as the result of kink-instability. Leighton (1969) was the first to note that kinking of a twisted flux tube may form a tilted pattern that can explain the axial tilt of active regions. This idea was observationally explored by several researchers as described in Section 6.6. The presence of non-zero twist (helicity) in flux tubes forming active regions may explain why active region tilt does not relax to a purely East-West direction. Longcope et al. (1999) compared the amplitude of twist (helicity proxy α coefficient) derived from the observations of vector magnetic field in the photosphere with the estimated contribution from different mechanisms, and concluded that majority of helicity originates from the interaction of magnetic flux tubes with turbulent convection (Σ-effect). The contribution of subphotospheric (interface) dynamo is minor. While the Σ-effect only "creates" helicity in the upper portion of a flux tube, the amount of this injected helicity is sufficient to explain statistical properties of Joy's law. Other mechanism of helicity injection into rising flux tube was recently proposed by Wang (2013), who considered the effects of the Coriolis force separately on each foot-point (sunspot) of rising flux tube. He concluded that as the flux tube foot-points expand, the action of the Coriolis force will inject helicity in each foot-point independently. This mechanism could produce a strong hemispheric helicity rule.

7 Summary

As magnetic field propagates from the dynamo region, evolves and dissipates, its changes also reflect the transport of helicity through solar interior and upper atmosphere. While helicity does not play a major role in all solar processes, it may affect many important processes from dynamo, magnetic reconnection, stability of magnetic systems and their eruption. In respect to tilt of active regions (Joy's law), the presence of non-zero helicity may explain why in their evolution, active regions evolve to a mean tilt (but not to a zero tilt), or why active regions at equatorial areas may still exhibit non-zero tilt. It seems

that helicity concept adds an additional level of "fine detail" to many solar processes, and this level of details requires considering the solar magnetic fields as a unified system, not as a collection of unrelated features. As such, potentially the concept of helicity may bring a much better understanding of "how our nearest star works."

Acknowledgements The National Solar Observatory (NSO) is operated by the Association of Universities for Research in Astronomy, AURA Inc under cooperative agreement with the National Science Foundation (NSF). AN's research has been partly co-financed by the European Union (European Social Fund -ESF) and Greek national funds through the Operational Program "Education and Lifelong Learning" of the National Strategic Reference Framework (NSRF) -Research Funding Program: "Thales. Investing in knowledge society through the European Social Fund". Data used in figure 9 were acquired by SOLIS instruments operated by NISP/NSO/AURA/NSF.

References

V.I. Abramenko, T. Wang, V.B. Yurchishin, Analysis of Electric Current Helicity in Active Regions on the Basis of Vector Magnetograms. Solar Phys. **168**, 75–89 (1996). doi:10.1007/BF00145826

V.I. Abramenko, T. Wang, V.B. Yurchishin, Electric Current Helicity in 40 Active Regions in the Maximum of Solar Cycle 22. Solar Phys. **174**, 291–296 (1997). doi:10.1023/A:1004957515498

T. Amari, J.F. Luciani, J.J. Aly, Z. Mikic, J. Linker, Coronal Mass Ejection: Initiation, Magnetic Helicity, and Flux Ropes. I. Boundary Motion-driven Evolution. Astrophys. J. **585**, 1073–1086 (2003a). doi:10.1086/345501

T. Amari, J.F. Luciani, J.J. Aly, Z. Mikic, J. Linker, Coronal Mass Ejection: Initiation, Magnetic Helicity, and Flux Ropes. II. Turbulent Diffusion-driven Evolution. Astrophys. J. **595**, 1231–1250 (2003b). doi:10.1086/377444

S.K. Antiochos, C.R. DeVore, J.A. Klimchuk, A Model for Solar Coronal Mass Ejections. Astrophys. J. **510**, 485–493 (1999). doi:10.1086/306563

G. Attrill, M.S. Nakwacki, L.K. Harra, L. van Driel-Gesztelyi, C.H. Mandrini, S. Dasso, J. Wang, Using the Evolution of Coronal Dimming Regions to Probe the Global Magnetic Field Topology. Solar Phys. **238**, 117–139 (2006). doi:10.1007/s11207-006-0167-5

H.W. Babcock, The Topology of the Sun's Magnetic Field and the 22-YEAR Cycle. Astrophys. J. **133**, 572 (1961). doi:10.1086/147060

S. Bao, H. Zhang, Patterns of Current Helicity for the Twenty-second Solar Cycle. Astrophys. J. Letters **496**, 43 (1998). doi:10.1086/311232

S.D. Bao, A.A. Pevtsov, T.J. Wang, H.Q. Zhang, Helicity Computation Using Observations From two Different Polarimetric Instruments. Solar Phys. **195**, 75–87 (2000). doi:10.1023/A:1005244700895

I. Baumann, D. Schmitt, M. Schüssler, S.K. Solanki, Evolution of the large-scale magnetic field on the solar surface: A parameter study. Astron. Astrophys. **426**, 1075–1091 (2004). doi:10.1051/0004-6361:20048024

M.A. Berger, Structure and stability of constant-alpha force-free fields. Astrophys. J. Supp. **59**, 433–444 (1985). doi:10.1086/191079

M.A. Berger, G.B. Field, The topological properties of magnetic helicity. Jour. Fluid Mechanics **147**, 133–148 (1984)

M.A. Berger, C. Prior, The writhe of open and closed curves. Journal of Physics A Mathematical General **39**, 8321–8348 (2006). doi:10.1088/0305-4470/39/26/005

M.A. Berger, A. Ruzmaikin, Rate of helicity production by solar rotation. Jour. Geophys. Res. **105**, 10481–10490 (2000). doi:10.1029/1999JA900392

M.A. Berger, Magnetic Helicity in Space Physics. Washington DC American Geophysical Union Geophysical Monograph Series **111**, 1–11 (1999)

M.A. Berger, Rigorous new limits on magnetic helicity dissipation in the solar corona. Geophys. Astrophys. Fluid Dynamics **30**(1-2), 79–104 (1984). doi:10.1080/03091928408210078. http://www.tandfonline.com/doi/abs/10.1080/03091928408210078

P.N. Bernasconi, D.M. Rust, D. Hakim, Advanced Automated Solar Filament Detection And Characterization Code: Description, Performance, And Results. Solar Phys. **228**, 97–117 (2005). doi:10.1007/s11207-005-2766-y

A. Brandenburg, C. Sandin, Catastrophic alpha quenching alleviated by helicity flux and shear. Astron. Astrophys. **427**, 13–21 (2004). doi:10.1051/0004-6361:20047086

M.T. Brown, R.C. Canfield, A.A. Pevtsov (eds.), Magnetic Helicity in Space abnd Laboratory Plasmas, in *Geophysical Monograph* (AGU, Washington, D. C., 1999)

W. Brunner, Gesetzmäßigkeiten in der Anordnung der Sonnenflecken zu Gruppen. Astronomische Mitteilungen der Eidgenössischen Sternwarte Zurich **13**, 67–78 (1930)

J. Büchner, A.A. Pevtsov (eds.), Magnetic Helicity at the Sun, in Solar Wind and Magnetospheres, in *Advances in Space Research*, vol. 32 (Elsevier, ???, 2003)

A.B. Burnette, R.C. Canfield, A.A. Pevtsov, Photospheric and Coronal Currents in Solar Active Regions. Astrophys. J. **606**, 565–570 (2004). doi:10.1086/382775

P.S. Cally, M. Dikpati, P.A. Gilman, Clamshell and Tipping Instabilities in a Two-dimensional Magnetohydrodynamic Tachocline. Astrophys. J. **582**, 1190–1205 (2003). doi:10.1086/344746

R.C. Canfield, A.A. Pevtsov, Helicity of Solar Active-Region Magnetic Fields, in *Synoptic Solar Physics*, ed. by K.S. Balasubramaniam, J. Harvey, D. Rabin Astronomical Society of the Pacific Conference Series, vol. 140, 1998, p. 131

J. Chae, Observational Determination of the Rate of Magnetic Helicity Transport through the Solar Surface via the Horizontal Motion of Field Line Footpoints. Astrophys. J. Letters **560**, 95–98 (2001). doi:10.1086/324173

J. Chae, Y.-J. Moon, Y.-D. Park, Determination of magnetic helicity content of solar active regions from SOHO/MDI magnetograms. Solar Phys. **223**, 39–55 (2004). doi:10.1007/s11207-004-0938-9

P. Charbonneau, Dynamo Models of the Solar Cycle. Living Reviews in Solar Physics **2**, 2 (2005)

A.R. Choudhuri, On the Connection Between Mean Field Dynamo Theory and Flux Tubes. Solar Phys. **215**, 31–55 (2003). doi:10.1023/A:1024874816178

A.R. Choudhuri, P. Chatterjee, D. Nandy, Helicity of Solar Active Regions from a Dynamo Model. Astrophys. J. Letters **615**, 57–60 (2004). doi:10.1086/426054

Călugăreanu, On isotopy classes of three dimensional knots and their invariants. Czechoslovak Math. J. **11**, 588–625 (1961)

K. Dalmasse, E. Pariat, G. Valori, P. Démoulin, L.M. Green, First observational application of a connectivity-based helicity flux density. Astron. Astrophys. **555**, 6 (2013). doi:10.1051/0004-6361/201321999

K. Dalmasse, E. Pariat, P. Démoulin, G. Aulanier, Photospheric Injection of Magnetic Helicity: Connectivity-Based Flux Density Method. Solar Phys. **289**, 107–136 (2014). doi:10.1007/s11207-013-0326-4

M. Dasi-Espuig, S.K. Solanki, N.A. Krivova, R. Cameron, T. Peñuela, Sunspot group tilt angles and the strength of the solar cycle. Astron. Astrophys. **518**, 7 (2010). doi:10.1051/0004-6361/201014301

M. Dasi-Espuig, S.K. Solanki, N.A. Krivova, R. Cameron, T. Peñuela, Sunspot group tilt angles and the strength of the solar cycle (Corrigendum). Astron. Astrophys. **556**, 3 (2013). doi:10.1051/0004-6361/201014301e

P. Démoulin, A review of the quantitative links between CMEs and magnetic clouds. Annales Geophysicae **26**, 3113–3125 (2008). doi:10.5194/angeo-26-3113-2008

P. Démoulin, M.A. Berger, Magnetic Energy and Helicity Fluxes at the Photospheric Level. Solar Phys. **215**, 203–215 (2003). doi:10.1023/A:1025679813955

P. Démoulin, E. Pariat, M.A. Berger, Basic properties of mutual magnetic helicity. Solar Phys. **233**, 3–27 (2006)

P. Démoulin, C.H. Mandrini, L. Van Driel-Gesztelyi, M.C. Lopez Fuentes, G. Aulanier, The Magnetic Helicity Injected by Shearing Motions. Solar Phys. **207**, 87–110 (2002a). doi:10.1023/A:1015531804337

P. Démoulin, C.H. Mandrini, L. van Driel-Gesztelyi, B.J. Thompson, S. Plunkett, Z. Kovári, G. Aulanier, A. Young, What is the source of the magnetic helicity shed by CMEs? The long-term helicity budget of AR 7978. Astron. Astrophys. **382**, 650–665 (2002b). doi:10.1051/0004-6361:20011634

C.R. DeVore, Magnetic Helicity Generation by Solar Differential Rotation. Astrophys. J. **539**, 944–953 (2000). doi:10.1086/309274

S. D'Silva, A.R. Choudhuri, A theoretical model for tilts of bipolar magnetic regions. Astron. Astrophys. **272**, 621 (1993)

Y. Fan, G.H. Fisher, A.N. McClymont, Dynamics of emerging active region flux loops. Astrophys. J. **436**, 907–928 (1994). doi:10.1086/174967

J.M. Finn, T.M. Antonsen Jr., Turbulent relaxation of compressible plasmas with flow. Physics of Fluids **26**, 3540–3552 (1983). doi:10.1063/1.864115

G.H. Fisher, Y. Fan, R.F. Howard, Comparisons between theory and observation of active region tilts. Astrophys. J. **438**, 463–471 (1995). doi:10.1086/175090

C. Foullon, C.J. Owen, S. Dasso, L.M. Green, I. Dandouras, H.A. Elliott, A.N. Fazakerley, Y.V. Bogdanova, N.U. Crooker, Multi-spacecraft study of the 21 january 2005 icme. Solar Physics **244**(1-2), 139–165 (2007). doi:10.1007/s11207-007-0355-y. http://dx.doi.org/10.1007/s11207-007-0355-y

M.K. Georgoulis, B.J. LaBonte, Reconstruction of an Inductive Velocity Field Vector from Doppler Motions and a Pair of Solar Vector Magnetograms. Astrophys. J. **636**, 475–495 (2006). doi:10.1086/497978

M.K. Georgoulis, B.J. LaBonte, Magnetic Energy and Helicity Budgets in the Active Region Solar Corona. I. Linear Force-Free Approximation. Astrophys. J. **671**, 1034–1050 (2007). doi:10.1086/521417

M.K. Georgoulis, K. Tziotziou, N.-E. Raouafi, Magnetic Energy and Helicity Budgets in the Active-region Solar Corona. II. Nonlinear Force-free Approximation. Astrophys. J. **759**, 1 (2012). doi:10.1088/0004-637X/759/1/1

M.K. Georgoulis, D.M. Rust, A.A. Pevtsov, P.N. Bernasconi, K.M. Kuzanyan, Solar Magnetic Helicity Injected into the Heliosphere: Magnitude, Balance, and Periodicities Over Solar Cycle 23. Astrophys. J. Letters **705**, 48–52 (2009). doi:10.1088/0004-637X/705/1/L48

P.A. Gilman, M. Dikpati, Joint Instability of Latitudinal Differential Rotation and Concentrated Toroidal Fields below the Solar Convection Zone. II. Instability of Narrow Bands at All Latitudes. Astrophys. J. **528**, 552–572 (2000). doi:10.1086/308146

P.A. Gilman, P.A. Fox, Joint Instability of Latitudinal Differential Rotation and Toroidal Magnetic Fields below the Solar Convection Zone. Astrophys. J. **484**, 439 (1997). doi:10.1086/304330

S. Gosain, A.A. Pevtsov, G.V. Rudenko, S.A. Anfinogentov, First Synoptic Maps of Photospheric Vector Magnetic Field from SOLIS/VSM: Non-radial Magnetic Fields and Hemispheric Pattern of Helicity. Astrophys. J. **772**, 52 (2013). doi:10.1088/0004-637X/772/1/52

L.M. Green, M.C. López fuentes, C.H. Mandrini, P. Démoulin, L. Van Driel-Gesztelyi, J.L. Culhane, The Magnetic Helicity Budget of a cme-Prolific Active Region. Solar Phys. **208**, 43–68 (2002). doi:10.1023/A:1019658520033

L.M. Green, B. Kliem, T. Török, L. van Driel-Gesztelyi, G.D.R. Attrill, Transient Coronal Sigmoids and Rotating Erupting Flux Ropes. Solar Phys. **246**, 365–391 (2007). doi:10.1007/s11207-007-9061-z

A.M. Gulisano, S. Dasso, C.H. Mandrini, P. Démoulin, Magnetic clouds: A statistical study of magnetic helicity. Journal of Atmospheric and Solar-Terrestrial Physics **67**, 1761–1766 (2005). doi:10.1016/j.jastp.2005.02.026

M. Hagino, T. Sakurai, Latitude Variation of Helicity in Solar Active Regions. Pub. Astron. Soc. Japan **56**, 831–843 (2004). doi:10.1093/pasj/56.5.831

M. Hagino, T. Sakurai, Solar-Cycle Variation of Magnetic Helicity in Active Regions. Pub. Astron. Soc. Japan **57**, 481–485 (2005). doi:10.1093/pasj/57.3.481

M.J. Hagyard, A.A. Pevtsov, Studies of Solar Helicity Using Vector Magnetograms. Solar Phys. **189**, 25–43 (1999). doi:10.1023/A:1005215001514

G.E. Hale, The Fields of Force in the Atmosphere of the Sun. Nature **119**, 708–714 (1927). doi:10.1038/119708a0

G.E. Hale, F. Ellerman, S.B. Nicholson, A.H. Joy, The Magnetic Polarity of Sun-Spots. Astrophys. J. **49**, 153 (1919). doi:10.1086/142452

J. Hao, M. Zhang, Hemispheric Helicity Trend for Solar Cycle 24. Astrophys. J. Letters **733**, 27 (2011). doi:10.1088/2041-8205/733/2/L27

Z.A. Holder, R.C. Canfield, R.A. McMullen, D. Nandy, R.F. Howard, A.A. Pevtsov, On the Tilt and Twist of Solar Active Regions. Astrophys. J. **611**, 1149–1155 (2004). doi:10.1086/422247

R.F. Howard, Axial tilt angles of sunspot groups. Solar Phys. **136**, 251–262 (1991). doi:10.1007/BF00146534

R.F. Howard, Axial Tilt Angles of Active Regions. Solar Phys. **169**, 293–301 (1996). doi:10.1007/BF00190606

V.G. Ivanov, Joy's law and its features according to the data of three sunspot catalogs. Geomagnetism and Aeronomy **52**, 999–1004 (2012). doi:10.1134/S0016793212080130

C. Jacobs, S. Poedts, B. van der Holst, The effect of the solar wind on CME triggering by magnetic foot point shearing. Astron. Astrophys. **450**, 793–803 (2006). doi:10.1051/0004-6361:20054670

B. Kliem, S. Rust, N. Seehafer, Helicity transport in a simulated coronal mass ejection, in *IAU Symposium*, ed. by A. Bonanno, E. de Gouveia Dal Pino, A.G. Kosovichev IAU Symposium, vol. 274, 2011, pp. 125–128. doi:10.1017/S1743921311006715

B. Kliem, T. Török, W.T. Thompson, A Parametric Study of Erupting Flux Rope Rotation. Modeling the "Cartwheel CME" on 9 April 2008. Solar Phys. **281**, 137–166 (2012). doi:10.1007/s11207-012-9990-z

A.G. Kosovichev, J.O. Stenflo, Tilt of Emerging Bipolar Magnetic Regions on the Sun. Astrophys. J. Letters **688**, 115–118 (2008). doi:10.1086/595619

K. Kusano, T. Maeshiro, T. Yokoyama, T. Sakurai, Measurement of Magnetic Helicity Injection and Free Energy Loading into the Solar Corona. Astrophys. J. **577**, 501–512 (2002). doi:10.1086/342171

K. Kusano, T. Yokoyama, T. Maeshiro, T. Sakurai, Annihilation of magnetic helicity: A new model for solar flare onset. Advances in Space Research **32**, 1931–1936 (2003). doi:10.1016/S0273-1177(03)90628-4

K. Kusano, T. Maeshiro, T. Yokoyama, T. Sakurai, The Trigger Mechanism of Solar Flares in a Coronal Arcade with Reversed Magnetic Shear. Astrophys. J. **610**, 537–549 (2004). doi:10.1086/421547

B.J. LaBonte, M.K. Georgoulis, D.M. Rust, Survey of Magnetic Helicity Injection in Regions Producing X-Class Flares. Astrophys. J. **671**, 955–963 (2007). doi:10.1086/522682

R.J. Leamon, R.C. Canfield, A.A. Pevtsov, Properties of magnetic clouds and geomagnetic storms associated with eruption of coronal sigmoids. Journal of Geophysical Research (Space Physics) **107**, 1234 (2002). doi:10.1029/2001JA000313

R.B. Leighton, A Magneto-Kinematic Model of the Solar Cycle. Astrophys. J. **156**, 1 (1969). doi:10.1086/149943

J. Li, R.K. Ulrich, Long-term Measurements of Sunspot Magnetic Tilt Angles. Astrophys. J. **758**, 115 (2012). doi:10.1088/0004-637X/758/2/115

E.-K. Lim, J. Chae, Chirality of Intermediate Filaments and Magnetic Helicity of Active Regions. Astrophys. J. **692**, 104–108 (2009). doi:10.1088/0004-637X/692/1/104

E.-K. Lim, H. Jeong, J. Chae, Y.-J. Moon, A Check for Consistency between Different Magnetic Helicity Measurements Based on the Helicity Conservation Principle. Astrophys. J. **656**, 1167–1172 (2007). doi:10.1086/510575

Y. Liu, P.W. Schuck, Magnetic Energy and Helicity in Two Emerging Active Regions in the Sun. Astrophys. J. **761**, 105 (2012). doi:10.1088/0004-637X/761/2/105

Y. Liu, P.W. Schuck, A Note on Computation of Relative Magnetic-Helicity Flux Across the Photosphere. Solar Phys. **283**, 283–294 (2013). doi:10.1007/s11207-012-0219-y

Y. Liu, J.T. Hoeksema, X. Sun, Test of the Hemispheric Rule of Magnetic Helicity in the Sun Using the Helioseismic and Magnetic Imager (HMI) Data. Astrophys. J. Letters **783**, 1 (2014). doi:10.1088/2041-8205/783/1/L1

D.W. Longcope, Inferring a Photospheric Velocity Field from a Sequence of Vector Magnetograms: The Minimum Energy Fit. Astrophys. J. **612**, 1181–1192 (2004). doi:10.1086/422579

D.W. Longcope, G.H. Fisher, The Effects of Convection Zone Turbulence on the Tilt Angles

of Magnetic Bipoles. Astrophys. J. **458**, 380 (1996). doi:10.1086/176821

D.W. Longcope, A. Malanushenko, Defining and calculating self-helicity in coronal magnetic fields. The Astrophysical Journal **674**(2), 1130 (2008). http://stacks.iop.org/0004-637X/674/i=2/a=1130

D.W. Longcope, B.T. Welsch, A Model for the Emergence of a Twisted Magnetic Flux Tube. Astrophys. J. **545**, 1089–1100 (2000). doi:10.1086/317846

D.W. Longcope, G.H. Fisher, A.A. Pevtsov, Flux-Tube Twist Resulting from Helical Turbulence: The Sigma-Effect. Astrophys. J. **507**, 417–432 (1998). doi:10.1086/306312

D.W. Longcope, M.G. Linton, A.A. Pevtsov, G.H. Fisher, I. Klapper, Twisted flux tubes and how they get that way, in *Magnetic Helicity in Space and Laboratory Plasmas*, ed. by M.R. Brown, R.C. Canfield, A.A. Pevtsov Geophysical Monographs Series, vol. 111 (AGU, Washington, D.C., 1999), pp. 93–101

M.C. López Fuentes, P. Démoulin, C.H. Mandrini, L. van Driel-Gesztelyi, The Counterkink Rotation of a Non-Hale Active Region. Astrophys. J. **544**, 540–549 (2000). doi:10.1086/317180

M.C. López Fuentes, P. Démoulin, C.H. Mandrini, A.A. Pevtsov, L. van Driel-Gesztelyi, Magnetic twist and writhe of active regions. On the origin of deformed flux tubes. Astron. Astrophys. **397**, 305–318 (2003). doi:10.1051/0004-6361:20021487

B.C. Low, Solar Activity and the Corona. Solar Phys. **167**, 217–265 (1996). doi:10.1007/BF00146338

B.C. Low, Magnetic helicity in a two-flux partitioning of an ideal hydromagnetic fluid. The Astrophysical Journal **646**(2), 1288 (2006). http://stacks.iop.org/0004-637X/646/i=2/a=1288

B.C. Low, M. Zhang, The Hydromagnetic Origin of the Two Dynamical Types of Solar Coronal Mass Ejections. Astrophys. J. Letters **564**, 53–56 (2002). doi:10.1086/338798

M.L. Luoni, P. Démoulin, C.H. Mandrini, L. van Driel-Gesztelyi, Twisted Flux Tube Emergence Evidenced in Longitudinal Magnetograms: Magnetic Tongues. Solar Phys. **270**, 45–74 (2011). doi:10.1007/s11207-011-9731-8

P. MacNeice, S.K. Antiochos, A. Phillips, D.S. Spicer, C.R. DeVore, K. Olson, A Numerical Study of the Breakout Model for Coronal Mass Ejection Initiation. Astrophys. J. **614**, 1028–1041 (2004). doi:10.1086/423887

C.H. Mandrini, S. Pohjolainen, S. Dasso, L.M. Green, P. Démoulin, L. van Driel-Gesztelyi, C. Copperwheat, C. Foley, Interplanetary flux rope ejected from an X-ray bright point. The smallest magnetic cloud source-region ever observed. Astron. Astrophys. **434**, 725–740 (2005). doi:10.1051/0004-6361:20041079

C.H. Mandrini, M.S. Nakwacki, G. Attrill, L. van Driel-Gesztelyi, P. Démoulin, S. Dasso, H. Elliott, Are CME-Related Dimmings Always a Simple Signature of Interplanetary Magnetic Cloud Footpoints? Solar Phys. **244**, 25–43 (2007). doi:10.1007/s11207-007-9020-8

S.F. Martin, Observational Criteria for Filament Models, in *Solar Active Region Evolution: Comparing Models with Observations*, ed. by K.S. Balasubramaniam, G.W. Simon Astronomical Society of the Pacific Conference Series, vol. 68, 1994, p. 264

S.F. Martin, Conditions for the Formation and Maintenance of Filaments (Invited Review). Solar Phys. **182**, 107–137 (1998). doi:10.1023/A:1005026814076

S.F. Martin, R. Billamoria, P.W. Tracadas, none known, in *Solar surface magnetism*, ed. by R.J. Rutten, C.J. Schrijver (Kluwer, ???, 1994), p. 303

S.F. Martin, O. Panasenco, M.A. Berger, O. Engvold, Y. Lin, A.A. Pevtsov, N. Srivastava, The Build-Up to Eruptive Solar Events Viewed as the Development of Chiral Systems, in *Second ATST-EAST Meeting: Magnetic Fields from the Photosphere to the Corona.*, ed. by T.R. Rimmele, A. Tritschler, F. Wöger, M. Collados Vera, H. Socas-Navarro, R. Schlichenmaier, M. Carlsson, T. Berger, A. Cadavid, P.R. Gilbert, P.R. Goode, M. Knölker Astronomical Society of the Pacific Conference Series, vol. 463, 2012, p. 157

B.H. McClintock, A.A. Norton, Recovering Joy's Law as a Function of Solar Cycle, Hemisphere, and Longitude. Solar Phys. **287**, 215–227 (2013). doi:10.1007/s11207-013-0338-0

H.K. Moffatt, The degree of knottedness of tangled vortex lines. Jour. Fluid Mechanics **35**, 117 (1969)

H.K. Moffatt, R.L. Ricca, Helicity and the Calugareanu Invariant. Royal Society of London Proceedings Series A **439**, 411–429 (1992). doi:10.1098/rspa.1992.0159

Y.-J. Moon, J. Chae, G.S. Choe, H. Wang, Y.D. Park, H.S. Yun, V. Yurchyshyn, P.R. Goode, Flare Activity and Magnetic Helicity Injection by Photospheric Horizontal Motions. Astrophys. J. **574**, 1066–1073 (2002a). doi:10.1086/340975

Y.-J. Moon, J. Chae, H. Wang, G.S. Choe, Y.D. Park, Impulsive Variations of the Magnetic Helicity Change Rate Associated with Eruptive Flares. Astrophys. J. **580**, 528–537 (2002b). doi:10.1086/343130

R.L. Moore, A.C. Sterling, H.S. Hudson, J.R. Lemen, Onset of the Magnetic Explosion in Solar Flares and Coronal Mass Ejections. Astrophys. J. **552**, 833–848 (2001). doi:10.1086/320559

D. Nandy, Magnetic helicity and flux tube dynamics in the solar convection zone: Comparisons between observation and theory. Journal of Geophysical Research (Space Physics) **111**(A10), 12 (2006). doi:10.1029/2006JA011882

A. Nindos, M.D. Andrews, The Association of Big Flares and Coronal Mass Ejections: What Is the Role of Magnetic Helicity? Astrophys. J. Letters **616**, 175–178 (2004). doi:10.1086/426861

A. Nindos, H. Zhang, Photospheric Motions and Coronal Mass Ejection Productivity. Astrophys. J. Letters **573**, 133–136 (2002). doi:10.1086/341937

A. Nindos, S. Patsourakos, T. Wiegelmann, On the Role of the Background Overlying Magnetic Field in Solar Eruptions. Astrophys. J. Letters **748**, 6 (2012). doi:10.1088/2041-8205/748/1/L6

A. Nindos, J. Zhang, H. Zhang, The Magnetic Helicity Budget of Solar Active Regions and Coronal Mass Ejections. Astrophys. J. **594**, 1033–1048 (2003). doi:10.1086/377126

A.A. Norton, P.A. Gilman, Recovering Solar Toroidal Field Dynamics from Sunspot Location Patterns. Astrophys. J. **630**, 1194–1205 (2005). doi:10.1086/431961

L.J. November, G.W. Simon, Precise proper-motion measurement of solar granulation. Astrophys. J. **333**, 427–442 (1988). doi:10.1086/166758

S. Ortolani, D.D. Schnack, *Magnetohydrodynamics of Plasma Relaxation* (World Scientific, ???, 1993)

E. Pariat, P. Démoulin, M.A. Berger, Photospheric flux density of magnetic helicity. Astron. Astrophys. **439**, 1191–1203 (2005). doi:10.1051/0004-6361:20052663

E. Pariat, P. Démoulin, A. Nindos, How to improve the maps of magnetic helicity injection in active regions? Advances in Space Research **39**, 1706–1714 (2007). doi:10.1016/j.asr.2007.02.047

E. Pariat, A. Nindos, P. Démoulin, M.A. Berger, What is the spatial distribution of magnetic helicity injected in a solar active region? Astron. Astrophys. **452**, 623–630 (2006). doi:10.1051/0004-6361:20054643

G.J.D. Petrie, Evolution of Active and Polar Photospheric Magnetic Fields During the Rise of Cycle 24 Compared to Previous Cycles. Solar Phys. **281**, 577–598 (2012). doi:10.1007/s11207-012-0117-3

A.A. Pevtsov, Transequatorial Loops in the Solar Corona. Astrophys. J. **531**, 553–560 (2000). doi:10.1086/308467

A.A. Pevtsov, Sinuous Coronal Loops at the Sun, in *Multi-Wavelength Observations of Coronal Structure and Dynamics*, ed. by P.C.H. Martens, D.P. Cauffman COSPAR Colloquia Series, vol. 13 (Pergamon, Dordrecht, 2002), pp. 125–134

A.A. Pevtsov, Helicity Generation and Signature in the Solar Atmosphere, in *IAU Joint Discussion*. IAU Joint Discussion, vol. 3, 2003

A.A. Pevtsov, What helicity can tell us about solar magnetic fields. Journal of Astrophysics and Astronomy **29**, 49–56 (2008). doi:10.1007/s12036-008-0006-1

A.A. Pevtsov, K.S. Balasubramaniam, Helicity patterns on the sun. Advances in Space Research **32**, 1867–1874 (2003). doi:10.1016/S0273-1177(03)90620-X

A.A. Pevtsov, R.C. Canfield, Helicity of the Photospheric Magnetic Field, in *Magnetic Helicity in Space and Laboratory Plasmas*, ed. by M.R. Brown, R.C. Canfield, A.A. Pevtsov Geophysical Monographs Series, vol. 111 (AGU, Washington, D.C., 1999), pp. 103–110

A.A. Pevtsov, S.M. Latushko, Current Helicity of the Large-Scale Photospheric Magnetic Field. Astrophys. J. **528**, 999–1003 (2000). doi:10.1086/308227

A.A. Pevtsov, D.W. Longcope, NOAA 7926: A Kinked Omega-Loop? Astrophys. J. **508**, 908–915 (1998). doi:10.1086/306414

A.A. Pevtsov, D.W. Longcope, Origin of Helicity in the Quiet Sun, in *Advanced Solar*

Polarimetry – Theory, Observation, and Instrumentation, ed. by M. Sigwarth Astronomical Society of the Pacific Conference Series, vol. 236, 2001, p. 423

A.A. Pevtsov, D.W. Longcope, Helicity as the Ultimate Test to the Surface Dynamo Problem, in *New Solar Physics with Solar-B Mission*, ed. by K. Shibata, S. Nagata, T. Sakurai Astronomical Society of the Pacific Conference Series, vol. 369, 2007, p. 99

A.A. Pevtsov, N.L. Peregud, Electric currents in a unipolar sunspot. Washington DC American Geophysical Union Geophysical Monograph Series **58**, 161–165 (1990)

A.A. Pevtsov, K.S. Balasubramaniam, J.W. Rogers, Chirality of Chromospheric Filaments. Astrophys. J. **595**, 500–505 (2003). doi:10.1086/377339

A.A. Pevtsov, R.C. Canfield, S.M. Latushko, Hemispheric Helicity Trend for Solar Cycle 23. Astrophys. J. Letters **549**, 261–263 (2001). doi:10.1086/319179

A.A. Pevtsov, R.C. Canfield, A.N. McClymont, On the Subphotospheric Origin of Coronal Electric Currents. Astrophys. J. **481**, 973 (1997). doi:10.1086/304065

A.A. Pevtsov, R.C. Canfield, T.R. Metcalf, Patterns of helicity in solar active regions. Astrophys. J. **425**, 117–119 (1994). doi:10.1086/187324

A.A. Pevtsov, R.C. Canfield, T.R. Metcalf, Latitudinal variation of helicity of photospheric magnetic fields. Astrophys. J. Letters **440**, 109–112 (1995). doi:10.1086/187773

A.A. Pevtsov, V.M. Maleev, D.W. Longcope, Helicity Evolution in Emerging Active Regions. Astrophys. J. **593**, 1217–1225 (2003a). doi:10.1086/376733

A.A. Pevtsov, M.J. Hagyard, Z. Blehm, J.E. Smith, R.C. Canfield, T. Sakurai, M. Hagino, On a Cyclic Variation of the Hemispheric Helicity Rule., in *IAU Joint Discussion*. IAU Joint Discussion, vol. 3, 2003b

A.A. Pevtsov, R.C. Canfield, T. Sakurai, M. Hagino, On the Solar Cycle Variation of the Hemispheric Helicity Rule. Astrophys. J. **677**, 719–722 (2008). doi:10.1086/533435

A.A. Pevtsov, M. Berger, A. Nindos, A. Norton, L. van Driel-Gesztelyi, Magnetic Helicity, Tilt, and Twist, in *The Solar activity Cycle: Physical Causes and Consequences*, ed. by A. Balogh, H. Hudson, K. Petrovay, R. von Steiger Space Science Series of ISSI, vol. 53 (Springer, ???, 2014)

A.D. Phillips, P.J. MacNeice, S.K. Antiochos, The Role of Magnetic Helicity in Coronal Mass Ejections. Astrophys. J. Letters **624**, 129–132 (2005). doi:10.1086/430516

K.G. Puschmann, B. Ruiz Cobo, V. Martínez Pillet, The Electrical Current Density Vector in the Inner Penumbra of a Sunspot. Astrophys. J. Letters **721**, 58–61 (2010). doi:10.1088/2041-8205/721/1/L58

B. Ravindra, D.W. Longcope, W.P. Abbett, Inferring Photospheric Velocity Fields Using a Combination of Minimum Energy Fit, Local Correlation Tracking, and Doppler Velocity. Astrophys. J. **677**, 751–768 (2008). doi:10.1086/528363

R.L. Ricca, B. Nipoti, Gauss linking number revisited. J. Knot Theory Ram. **20**, 1325–1343 (2011)

P. Romano, F. Zuccarello, Flare occurrence and the spatial distribution of the magnetic helicity flux. Astron. Astrophys. **535**, 1–5 (2011). doi:10.1051/0004-6361/201117594

P. Romano, L. Contarino, F. Zuccarello, Eruption of a helically twisted prominence. Solar Phys. **214**, 313–323 (2003). doi:10.1023/A:1024257603143

G.V. Rudenko, I.I. Myshyakov, Gauge-Invariant Helicity for Force-Free Magnetic Fields in a Rectangular Box. Solar Phys. **270**, 165–173 (2011). doi:10.1007/s11207-011-9743-4

B. Ruiz Cobo, K.G. Puschmann, Twist, Writhe, and Helicity in the Inner Penumbra of a Sunspot. Astrophys. J. **745**, 141 (2012). doi:10.1088/0004-637X/745/2/141

D.M. Rust, Spawning and shedding helical magnetic fields in the solar atmosphere. Geophys. Res. Lett. **21**, 241–244 (1994). doi:10.1029/94GL00003

D.M. Rust, A. Kumar, Evidence for Helically Kinked Magnetic Flux Ropes in Solar Eruptions. Astrophys. J. Letters **464**, 199 (1996). doi:10.1086/310118

D.M. Rust, S.F. Martin, A Correlation Between Sunspot Whirls and Filament Type, in *Solar Active Region Evolution: Comparing Models with Observations*, ed. by K.S. Balasubramaniam, G.W. Simon Astronomical Society of the Pacific Conference Series, vol. 68, 1994, p. 337

H.U. Schmidt, Magnetohydrodynamics of an Active Region, in *Structure and Development of Solar Active Regions*, ed. by K.O. Kiepenheuer IAU Symposium, vol. 35, 1968, p. 95

P.W. Schuck, Tracking Vector Magnetograms with the Magnetic Induction Equation. Astrophys. J. **683**, 1134–1152 (2008). doi:10.1086/589434

M. Schüssler, P. Caligari, A. Ferriz-Mas, F. Moreno-Insertis, Instability and eruption of magnetic flux tubes in the solar convection zone. Astron. Astrophys. **281**, 69–72 (1994)
N. Seehafer, Electric current helicity in the solar atmosphere. Solar Phys. **125**, 219–232 (1990). doi:10.1007/BF00158402
K.R. Sivaraman, S.S. Gupta, R.F. Howard, Measurement of Kodaikanal white-light images - IV. Axial Tilt Angles of Sunspot Groups. Solar Phys. **189**, 69–83 (1999). doi:10.1023/A:1005277515551
J.O. Stenflo, A.G. Kosovichev, Bipolar Magnetic Regions on the Sun: Global Analysis of the SOHO/MDI Data Set. Astrophys. J. **745**, 129 (2012). doi:10.1088/0004-637X/745/2/129
J.K. Thalmann, B. Inhester, T. Wiegelmann, Estimating the Relative Helicity of Coronal Magnetic Fields. Solar Phys. **272**, 243–255 (2011). doi:10.1007/s11207-011-9826-2
J.K. Thalmann, S.K. Tiwari, T. Wiegelmann, Force-free field modeling of twist and braiding-induced magnetic energy in an active-region corona. Astrophys. J. **780**(1), 102 (2014). http://stacks.iop.org/0004-637X/780/i=1/a=102
L. Tian, Y. Liu, Tilt and alpha$_{best}$ of major flare-producing active regions. Astron. Astrophys. **407**, 13–16 (2003). doi:10.1051/0004-6361:20030977
L. Tian, S. Bao, H. Zhang, H. Wang, Relationship in sign between tilt and twist in active region magnetic fields. Astron. Astrophys. **374**, 294–300 (2001). doi:10.1051/0004-6361:20010701
A.G. Tlatov, A.A. Pevtsov, Bimodal Distribution of Magnetic Fields and Areas of Sunspots. Solar Phys. **289**, 1143–1152 (2014). doi:10.1007/s11207-013-0382-9
A.G. Tlatov, V.V. Vasil'eva, A.A. Pevtsov, Distribution of Magnetic Bipoles on the Sun over Three Solar Cycles. Astrophys. J. **717**, 357–362 (2010). doi:10.1088/0004-637X/717/1/357
T. Török, B. Kliem, Confined and Ejective Eruptions of Kink-unstable Flux Ropes. Astrophys. J. Letters **630**, 97–100 (2005). doi:10.1086/462412
T. Török, M.A. Berger, B. Kliem, The writhe of helical structures in the solar corona. Astron. Astrophys. **516**, 49 (2010). doi:10.1051/0004-6361/200913578
T. Török, B. Kliem, M.A. Berger, M.G. Linton, P. Demoulin, L. van Driel-Gesztelyi, The Evolution of Writhe in Kink-Unstable Flux Ropes and Erupting Filaments. Plasma Phys. Controlled Fusion **in press** (2014)
K. Tziotziou, M.K. Georgoulis, Y. Liu, Interpreting Eruptive Behavior in NOAA AR 11158 via the Region's Magnetic Energy and Relative-helicity Budgets. Astrophys. J. **772**, 115 (2013). doi:10.1088/0004-637X/772/2/115
K. Tziotziou, M.K. Georgoulis, N.-E. Raouafi, The Magnetic Energy-Helicity Diagram of Solar Active Regions. Astrophys. J. Letters **759**, 4 (2012). doi:10.1088/2041-8205/759/1/L4
L. Upton, D.H. Hathaway, Predicting the Sun's Polar Magnetic Fields with a Surface Flux Transport Model. Astrophys. J. **780**, 5 (2014). doi:10.1088/0004-637X/780/1/5
G. Valori, P. Démoulin, E. Pariat, Comparing Values of the Relative Magnetic Helicity in Finite Volumes. Solar Phys. **278**, 347–366 (2012). doi:10.1007/s11207-012-0044-3
A.A. van Ballegooijen, P.C.H. Martens, Formation and eruption of solar prominences. Astrophys. J. **343**, 971–984 (1989). doi:10.1086/167766
B. Vršnak, V. Ruždjak, B. Rompolt, Stability of prominences exposing helical-like patterns. Solar Phys. **136**, 151–167 (1991). doi:10.1007/BF00151701
C. Wang, M. Zhang, A Hemispheric Helicity Sign Rule Indicated by Large-scale Photospheric Magnetic Fields at Three Phases of Solar Cycle 23. Astrophys. J. **720**, 632–638 (2010). doi:10.1088/0004-637X/720/1/632
Y.-M. Wang, On the Strength of the Hemispheric Rule and the Origin of Active-region Helicity. Astrophys. J. Letters **775**, 46 (2013). doi:10.1088/2041-8205/775/2/L46
Y.-M. Wang, N.R. Sheeley Jr., Average properties of bipolar magnetic regions during sunspot cycle 21. Solar Phys. **124**, 81–100 (1989). doi:10.1007/BF00146521
Y.-M. Wang, N.R. Sheeley Jr., Magnetic flux transport and the sun's dipole moment - New twists to the Babcock-Leighton model. Astrophys. J. **375**, 761–770 (1991). doi:10.1086/170240
M.A. Weber, Y. Fan, M.S. Miesch, The Rise of Active Region Flux Tubes in the Turbulent Solar Convective Envelope. Astrophys. J. **741**, 11 (2011). doi:10.1088/0004-

637X/741/1/11
M.A. Weber, Y. Fan, M.S. Miesch, Comparing Simulations of Rising Flux Tubes Through the Solar Convection Zone with Observations of Solar Active Regions: Constraining the Dynamo Field Strength. Solar Phys. **287**, 239–263 (2013). doi:10.1007/s11207-012-0093-7
B.T. Welsch, D.W. Longcope, Magnetic Helicity Injection by Horizontal Flows in the Quiet Sun. I. Mutual-Helicity Flux. Astrophys. J. **588**, 620–629 (2003). doi:10.1086/368408
B.T. Welsch, G.H. Fisher, W.P. Abbett, S. Regnier, ILCT: Recovering Photospheric Velocities from Magnetograms by Combining the Induction Equation with Local Correlation Tracking. Astrophys. J. **610**, 1148–1156 (2004). doi:10.1086/421767
B.T. Welsch, W.P. Abbett, M.L. De Rosa, G.H. Fisher, M.K. Georgoulis, K. Kusano, D.W. Longcope, B. Ravindra, P.W. Schuck, Tests and Comparisons of Velocity-Inversion Techniques. Astrophys. J. **670**, 1434–1452 (2007). doi:10.1086/522422
D.R. Williams, T. Török, P. Démoulin, L. van Driel-Gesztelyi, B. Kliem, Eruption of a Kink-unstable Filament in NOAA Active Region 10696. Astrophys. J. Letters **628**, 163–166 (2005). doi:10.1086/432910
P.R. Wilson, R.C. Altrocki, K.L. Harvey, S.F. Martin, H.B. Snodgrass, The extended solar activity cycle. Nature **333**, 748–750 (1988). doi:10.1038/333748a0
A. Wright, M.A. Berger, The effect of reconnection upon the linkage and interior structure of magnetic flux tubes. Jour. Geophys. Res. **94**, 1295–1302 (1989)
S. Yang, H. Zhang, Large-scale Magnetic Helicity Fluxes Estimated from MDI Magnetic Synoptic Charts over the Solar Cycle 23. Astrophys. J. **758**, 61 (2012). doi:10.1088/0004-637X/758/1/61
A.R. Yeates, D.H. Mackay, A.A. van Ballegooijen, Modelling the Global Solar Corona: Filament Chirality Observations and Surface Simulations. Solar Phys. **245**, 87–107 (2007). doi:10.1007/s11207-007-9013-7
H. Zhang, T. Sakurai, A. Pevtsov, Y. Gao, H. Xu, D.D. Sokoloff, K. Kuzanyan, A new dynamo pattern revealed by solar helical magnetic fields. Monthly Notices Royal Astron. Soc. **402**, 30–33 (2010). doi:10.1111/j.1745-3933.2009.00793.x
M. Zhang, Helicity Observations of Weak and Strong Fields. Astrophys. J. Letters **646**, 85–88 (2006). doi:10.1086/506560
M. Zhang, N. Flyer, The Dependence of the Helicity Bound of Force-Free Magnetic Fields on Boundary Conditions. Astrophys. J. **683**, 1160–1167 (2008). doi:10.1086/589993
M. Zhang, B.C. Low, Magnetic Flux Emergence into the Solar Corona. I. Its Role for the Reversal of Global Coronal Magnetic Fields. Astrophys. J. **561**, 406–419 (2001). doi:10.1086/323238
M. Zhang, B.C. Low, Magnetic Flux Emergence into the Solar Corona. III. The Role of Magnetic Helicity Conservation. Astrophys. J. **584**, 479–496 (2003). doi:10.1086/345615
M. Zhang, B.C. Low, The Hydromagnetic Nature of Solar Coronal Mass Ejections. Ann. Rev. Astron. Astrophys. **43**, 103–137 (2005). doi:10.1146/annurev.astro.43.072103.150602
M. Zhang, N. Flyer, B. Chye Low, Magnetic Helicity of Self-similar Axisymmetric Force-free Fields. Astrophys. J. **755**, 78 (2012). doi:10.1088/0004-637X/755/1/78
M. Zhang, N. Flyer, B.C. Low, Magnetic Field Confinement in the Corona: The Role of Magnetic Helicity Accumulation. Astrophys. J. **644**, 575–586 (2006). doi:10.1086/503353
Y. Zhang, R. Kitai, K. Takizawa, Magnetic Helicity Transported by Flux Emergence and Shuffling Motions in Solar Active Region NOAA 10930. Astrophys. J. **751**, 85 (2012). doi:10.1088/0004-637X/751/2/85
F.P. Zuccarello, C. Jacobs, A. Soenen, S. Poedts, B. van der Holst, F. Zuccarello, Modelling the initiation of coronal mass ejections: magnetic flux emergence versus shearing motions. Astron. Astrophys. **507**, 441–452 (2009). doi:10.1051/0004-6361/200912541